Chapter 3. Detailed study of the event on June 6-7, 1989

As mentioned in the Chapter 2, auroral substorm event on June 6-7, 1989 was the most ideal and fortuitous event observed in 1989. In this Chapter, we will analyze this event in detail. Growth phase evolution is analyzed in the section 3.1, and expansion phase evolution is analyzed in the section 3.2.

3.1. Growth phase evolution of nightside auroral activities and ionospheric convection toward expansion phase onset: June 6-7, 1989 event

Abstract.

We have analyzed in detail the evolution of nightside auroral activities and ionospheric convection during the growth phase of an isolated substorm. The following three characteristic auroral activities were identified by meridian scanning photometers at ground stations: 1. proton main oval; 2. Fast Equatorward Moving (FEM) arc; 3. Near Plasma Sheet Boundary Layer (NPSBL) aurora. The proton main oval corresponds to the main part of the proton auroral region and was located at the equatorward-most region of the electron auroral emissions, and gradually moved equatorward during the growth phase. The FEM arc was a discrete auroral arc having a clear longitudinally elongated form. It appeared about 20 min before the onset on the high latitude side of the auroral region, and moved equatorward toward the proton main oval. Its equatorward motion gradually slowed as it approached the proton main oval. As the FEM arc moved equatorward, the location of the peak velocity in the nightside return flow of the two-cell convection also moved equatorward. The auroral breakup occurred in a localized area around the demarcation region between the two return flows, close to the latitude of the FEM arc. This was observed by the UV imager aboard the AKEBONO satellite. The NPSBL aurora appeared a few minutes before the onset around the poleward-most region of the aurora, and continued even after the onset. Our detailed analysis of these phenomena can give us important clues as to how the growth phase proceeds toward the expansion phase onset.

1. Introduction

A special stage in a substorm evolution, called the growth phase [*McPherron*, 1970], seems now widely accepted, though this concept has attracted some controversial [*e.g., Akasofu and Snyder*, 1972; *Kamide and Matsushita*, 1978; *McPherron*, 1994]. Growth phase features are most clearly seen in a substorm which starts after southward turning of the interplanetary magnetic field (IMF), preceded by a prolonged northward IMF period [*e.g., Shue et al.*, 2000]. The growth phase is considered to be a pre-conditioning phase for the expansion phase onset. One of the most debated topics concerns the onset mechanism for

substorm. For example, the relative timing of various onset signatures both in the magnetosphere and ionosphere, including formation of the near earth neutral line (NENL), cross-tail current disruption (CD), auroral breakup, and Pi2 onset, are critical issues concerning the onset mechanism [e.g., *Lui*, 2001]. Precise understanding of the growth phase evolution is important to know how and where the necessary conditions for the onset mechanism are set up. In this study, we have analyzed in detail the spatial and temporal relationship between auroral activities and other ionospheric phenomena during the growth phase of an isolated substorm. Although there were no observations in the magnetotail region beyond geosynchronous orbit, well-coordinated ionospheric observations give us an insight as to how the pre-conditioning proceeded toward the onset both in the ionosphere and magnetosphere. In the following paragraphs, we introduce several growth phase features which were observed and are discussed in this paper.

During the growth phase, both electron and proton auroral ovals on the nightside gradually move equatorward. This has been observed both from the ground [e.g., *Fukunishi*, 1975b; *Deehr*, 1994; *Deehr and Lummerzheim, 2001*; *Samson et al.*, 1992a; *Lyons et al.*, 1997] and from satellites [e.g., *Murphree et al.*, 1991; *Brittnacher et al.*, 1999]. Very often, the poleward boundary of the auroral oval moves more rapidly than its equatorward boundary, which results in a gradual decrease of the latitudinal width of the oval [*Brittnacher et al.*, 1999]. Such a variation of the auroral oval is considered to be associated with thinning of the plasma sheet and a configuration change of the magnetic field lines toward a more taillike geometry [e.g., *Kokubun and McPherron*, 1981; *Sergeev et al.*, 1990; *Sanny et al.*, 1994].

During the growth phase, the two-cell convection pattern, or DP-2 current system [*Nishida*, 1968], develops in the ionosphere and expands equatorward and from the dayside to the nightside. This is observed by the ground magnetometer networks as an evolution of the equivalent current system [e.g., Fig. 2a of *Kamide and Baumjohann*, 1985]. This enhancement in the ionospheric two-cell convection suggests an enhancement in the sunward convection in the tail. *Machida et al.* [2000] showed that activation of the earthward flow from the distant neutral line (DNL), which is located at around X = -130 Re, starts at least 20 min prior to the onset.

HF radar beam backscatter region also moves equatorward during the growth phase [e.g., *Lewis et al.*, 1998; *Voronkov et al.*, 1999]. *Voronkov et al.* [1999] analyzed the relationship among auroral activity, nightside ionospheric convection, and the HF radar backscatter region during the growth phase. They showed that the maximum of the westward flow, the lower latitude part of the evening-side convection cell, intensified and moved equatorward. This movement was following the proton auroral oval. They also showed that a significant latitudinal gradient in the convective flow developed within the proton aurora region prior to the onset.

As for the onset location, it seems to be generally accepted that the substorm expansive

phase often starts with a sudden brightening of an equatorward-most arc (hereinafter called the "onset arc") [*Akasofu*, 1964]. Hence the onset arc should be closely associated with the onset mechanism, although the generation mechanism of the onset arc and its role in the onset process are still unresolved problems [e.g., *Lyons and Samson*, 1992a; *Lui and Murphree*, 1998].

Based on ground observations, *Oguti* [1973] showed that, on many occasions, an electron sheet aurora splits from the highest latitude arc, moves equatorward, and eventually makes contact with the poleward boundary of the proton auroral region at lower latitude. Auroral breakup occurs at the contact. In contrast, *Deehr and Lummerzheim* [2001] showed that the peak hydrogen emission moves equatorward more quickly than does the onset arc. They also showed that the onset arc is located 10-300 km poleward of the peak proton precipitation, which is consistent with *Oguti* [1973]. Such a spatial relationship between the onset arc and proton auroral oval at the onset time has also been studied in other previous works [*Montbriand*, 1971; *Fukunishi*, 1975b; *Vallance Jones et al.*, 1982; *Samson et al.*, 1992a]. *Samson et al.* [1992a] showed that breakup occurs 4-6 deg equatorward from the open-closed field line boundary (hereinafter called the open/close boundary), estimated by the poleward edge of 630.0 nm emissions. Similar results were also shown by *Friedrich et al.* [2001].

The relationship of the onset arc with precipitating magnetospheric particles has also been studied using the observations by low altitude satellites. The onset arc was located between the CPS and BSP-type [cf. *Winningham et al.*, 1975] electron precipitation boundaries [*Lui and Burrows*, 1978]; near the electron trapping boundary [*Lui and Burrows*, 1978; *Persson et al.*, 1994a], and UV auroral brightening occurs in the middle of the main UV oval, poleward of the energetic proton isotropic boundary (IB) [*Elphinstone et al.*, 1995a].

All the above mentioned results suggest that onset location in the tail should be in the near earth region, around X=-5 to -15 Re, as shown in the tailward mapping of the auroral brightening region by *Pulkkinen et al.* [1991; 1992]. In the magnetosphere, current disruption, which is considered to be an onset signature, is frequently observed in the near earth region [e.g., *Lui*, 1996].

On the other hand, it is well-established from observations by GEOTAIL satellite that the NENL is actually formed during the substorm evolution [e.g., *Ieda et al.*, 1998], and its initial location should be around X=-20 to -30 Re [e.g., *Nagai et al.*, 1998; *Nagai and Machida*, 1998; *Machida et at.*, 1999; *Miyashita et al.*, 2000]. It is a critical issue whether formation of the NENL occurs before or after the expansion phase onset, although many event studies and statistical studies have shown that it often starts about 1 to 5 min before the ground-based Pi2 onset [e.g., *Sergeev et al.*, 1995; *Mukai et al.*, 1998; *Ohtani et al.*, 1999; *Nagai et al.*, 1998; *Nagai and Machida*, 1998; *Machida et at.*, 1999; *Miyashita et al.*, 2000]. *Lui et al.* [1998] claimed that there is no indication of strong flows (a signature of NENL formation) before the auroral breakup. To our knowledge, any possible ionospheric, especially auroral, signature of

the NENL formation before the onset has not yet been reported.

Other unresolved problems concerning the onset location are its pre-midnight preference and its localization. It is known that the initial auroral brightening tends to occur more frequently in the pre-midnight localized region [e.g., *Frank and Craven*, 1988; *Murphree et al.*, 1991; *Elphinstone et al.*, 1995a]. Such a pre-midnight preference was also observed in the magnetosphere for plasma injection [*Arnoldy and Moore*, 1983; *Lopez et al.*, 1990] and magnetic field dipolarization [*Nagai*, 1991] in the near earth region, and for initial formation of the NENL [e.g., *Machida et al.*, 1999; *Miyashita et al.*, 2000] and plasmoid formation [*Ieda et al.*, 1998] in the near and mid tail regions. Although such a pre-midnight preference and localization seem to be essential features of the onset phenomena, there have been few works to show how those features are established toward the onset.

In section 2, observational results are presented to show the growth phase evolution toward the onset. In section 3, we discuss the ionospheric and magnetospheric processes during the growth phase, based on these observations and previous studies. A summary of this study is presented in section 4.

2. Observations

2.1. Overview

This substorm occurred after a prolonged quiescent period. Figure 3.1.1 shows solar wind parameters observed by IMP-8 (upper 6 panels) and magnetic activity on the ground (bottom panel) from 14:00 UT on June 6 to 09:00 UT on June 7, 1989. IMP-8 was situated at (-25.2, 20.1, 25.5) Re in Geocentric Solar Magnetospheric (GSM) coordinates when a discontinuity in the solar wind parameters was observed at 23:16:20 UT on June 6, 1989. Ground stations recorded the geomagnetic sudden commencement (SC) at 23:14 UT [*Solar-Geophysical Data prompt reports*, No. 540, Part-1, 1989]. After the arrival of the discontinuity, both the dynamic and static pressures increased by about one order of magnitude, and the high-pressure state continued afterward. The IMF turned southward around 23:40 UT, and the southward condition continued until 02:27 UT on June 7. Geomagnetic activity was enhanced soon after the SC, substorm growth phase features appeared around the time of the IMF southward turning, and a substorm expansion phase onset occurred around 00:41:40 UT on June 7, as determined by Pi2 activity at the Hermanus (HER) station and global auroral activity observed by the UV auroral TV camera (ATV-UV) aboard AKEBONO satellite. Figure 3.1.2 shows the ATV-UV data showing auroral bulge evolution after the onset. ATV-UV observed the auroral activity over the Antarctic region from 00:37:28 UT until 01:05:00 UT from altitudes of 10,296 km - 9,947 km. As can be seen in Figures 3.1.1 and 3.1.2, a significant development of the substorm current system and a significant expansion of the auroral bulge were observed after the onset.

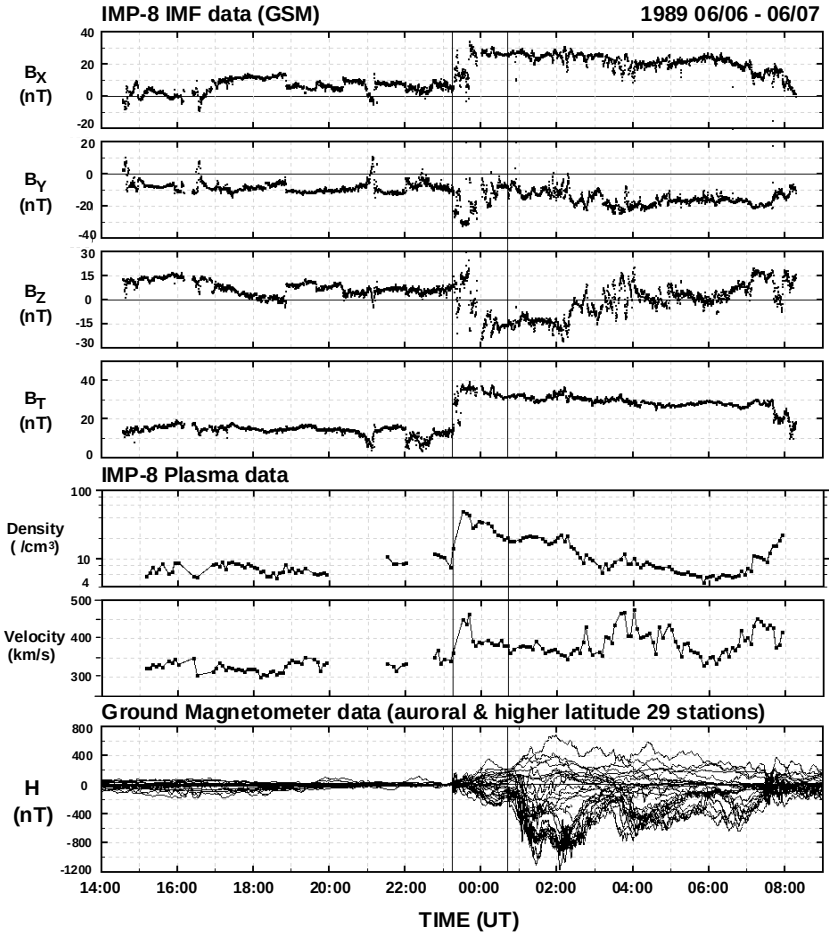

Figure 3.1.1. Solar wind condition and magnetic activity from 14:00 UT on June 6 to 09:00 UT on June 7, 1989. Upper 6 panels show solar wind parameters observed by IMP-8 satellite: GSM X, Y, Z-components; total magnitude of the magnetic field; plasma density and bulk velocity. Bottom panel: Magnetic variation in H (magnetic northward) component at auroral and higher latitude stations. Left and right vertical lines indicate the times of the SC and expansion phase onset of the substorm, respectively.

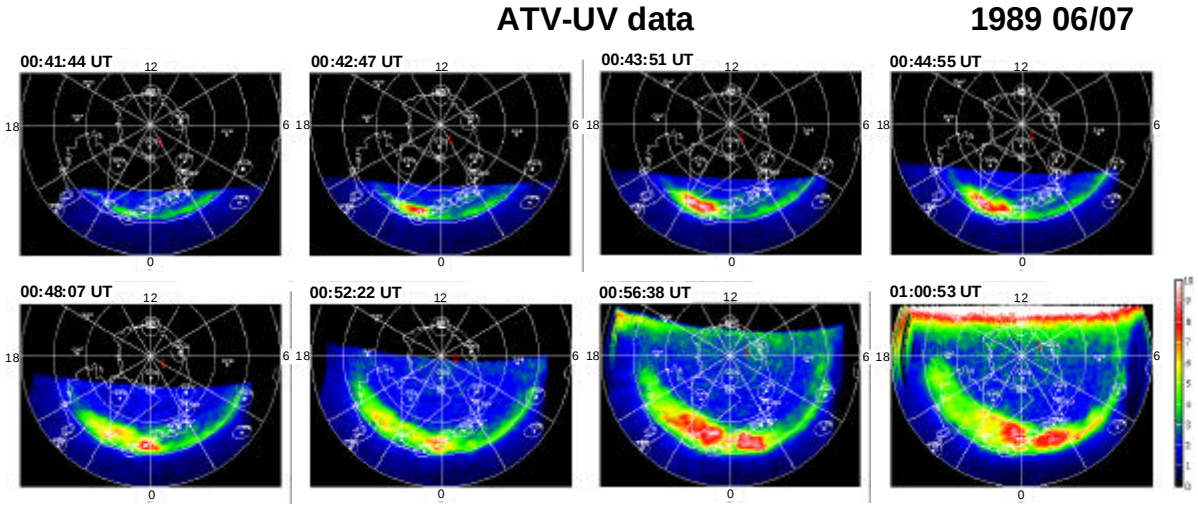

Figure 3.1.2. Four-frame averaged ATV-UV data from 00:41:44 UT to 01:00:53 UT on June 7, 1989, mapped to ILAT vs MLT polar coordinates at 120 km altitude. Time intervals for the top and bottom panels are 64 sec and 256 sec, respectively.

2.2. Instrumentation

Figure 3.1.3 shows the spatial relationship between the auroral breakup location and various observations analyzed in this study. ATV-UV data at 00:41:44 UT, when the first indication of breakup was observed, are shown on the southern hemisphere polar map at 120 km altitude in the invariant latitude (ILAT) and MLT coordinates. The auroral image is shown in a color code, as indicated by the color bar, where the relative emission intensity is linearly classified. The blue area distinguished from the black background indicates the field-of-view (FOV) of the ATV-UV. Breakup occurred near Sanae (SNA) station, and peak intensity of the brightened area was located at 62.7 deg ILAT and 22.9 hr MLT. Before the onset, footprints of three low altitude satellites, AKEBONO, NOAA-10 and DMSP-F9, traversed close to the breakup region, as shown in Fig. 3.1.3. Those footprints were calculated by the *Tsyganenko* [1989a] model with Kp=0 (T89(Kp=0)). Note that the orbit of the DMSP-F9 was in the northern hemisphere, while both AKEBONO and NOAA-10 were in the southern hemisphere. The trajectory of DMSP-F9 in Fig. 3.1.3 is drawn by tracing the model geomagnetic field-lines from the northern hemisphere. The footprints of geosynchronous satellites, GOES-7 (G07) and LANL-1987-097 (L87), calculated by the T89(Kp=0) model, are also shown in Fig. 3.1.3. The FOV of the HF-radar at Halley (HBA) station and the FOV of each station for the elevation above 20 deg are also shown.

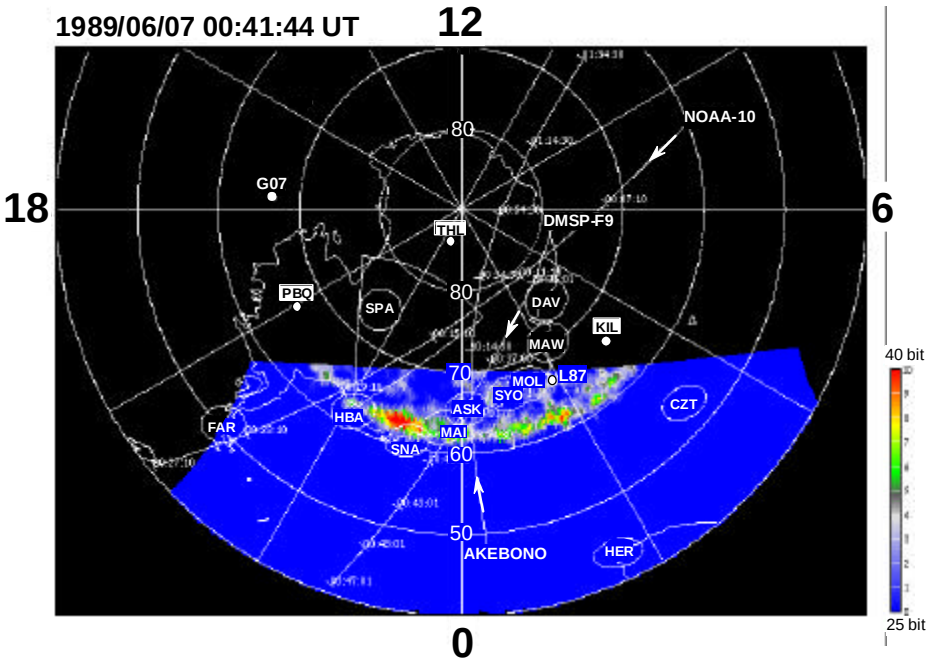

Figure 3.1.3. ATV-UV data at 00:41:44 UT projected on to a southern hemisphere map at 120 km altitude in the ILAT vs MLT coordinate. Footprints of geosynchronous satellites, GOES-7 (G07) and LANL-1987-097 (L87), and footprint trajectories of AKEBONO, NOAA-10 and DMSP-F9 satellites are also shown. Those footprints are calculated with the T89 (Kp=0) model. Conjugate locations of northern hemisphere stations, THL, PBQ and KIL, are also shown with white circles.

The ATV-UV is described in detail by *Oguti et al.* [1990]. It can take a snapshot image in the wave length range of 115.0-139.0 nm with its highest time resolution of the satellite spin period, about 8 sec. Its FOV is 36 deg x 36 deg and the center of the FOV is directed perpendicular to the satellite spin axis, which directs toward the sun. ATV-UV has several observational modes. During this event, the observational sequence was 8-8-8-40 sec. Hence, four images were taken successively at every satellite spin period, and the following 5 spin periods were necessary for transmission of the data. Pixel number of the CCD was 244 x 188 within the FOV, and the CCD charge accumulation time was set to 600 ms. AKEBONO was launched on February 22, 1989 into a semi-polar orbit with an initial apogee, perigee and inclination of, respectively, 10,500 km, 274 km and 75 deg, and with an evolution period of 212 min [*Oya and Tsuruda*, 1990].

A meridian scanning photometer (MSP) and a panchromatic all-sky SIT-TV camera were operated at Syowa (SYO) station during this event. At Asuka (ASK) station, only a MSP was operated. Syowa MSP observed emissions from the atomic oxygen (OI) green line (557.7 nm), red line (630.0 nm) and hydrogen Balmer-line (486.1 nm (Hß)) simultaneously. Its scanning speed was 180 deg/30 sec from horizon to horizon, its FOV was 3 deg for OI emissions and 5 deg for Hß emission, and its sampling rate was 1 Hz. A tilting filter technique similar to that of *Fukunishi* [1975b] was applied for the Hß observation, and the tilting frequency was 1 Hz. The intensity difference between the maximum and minimum outputs during the 1 sec tilting period was analyzed in this study for the Hß data. Effects of the air extinction and the van Rhijn are corrected. Due to a calibration failure, we cannot determine the absolute intensity for each auroral emission. Only the relative variation of each emission will be discussed in the following sections. Specifications of the Asuka MSP are almost the same as those of the Syowa MSP. Its sampling rate was 2 Hz. SIT-TV data were recorded on a videotape with the original video rate. Responsivity of the SIT-TV camera had a peak value around 427.8 nm.

The field of view of the Halley HF-radar consists of 16 beams with beam azimuthal separation of 3.24 deg. Beam numbers 0-15 are assigned from east to west; beam 8 is directed almost along the magnetic meridian at HBA. Each beam consisted of 50 range bins each of 45 km. The closest range was set to 585 km for the data on 6 June, 1989, and 135 km for the data on 7 June. The beam integration period was 6 sec; hence one full scan of the 16 beams required 96 sec. The HF-radar observes the line-of-sight (LOS) Doppler velocity of the field-aligned electron density irregularity, mainly in the F-region, which has been shown to be the plasma bulk velocity. Such an irregularity is considered to be produced by some instability [e.g., *Tsunoda*, 1988].

Fluxgate magnetometer data from the stations shown in Fig. 3.1.3 were also used, and induction magnetometer data were available at ASK, SYO, and HER.

2.3. Growth phase features

(1) Geosynchronous observation

Figure 3.1.4 shows the variation in the number flux of energetic electrons observed by L87 (top panel), and the variation in total intensity (middle panel) and polar angle (bottom panel) of the magnetic field observed by G07 in geosynchronous orbit. Left and right vertical lines indicate the times of SC and expansion phase onset, respectively. Magnetospheric compression associated with the SC was clearly seen in a sharp enhancement of the total magnetic field. Increase of the polar angle (taillike configuration change) started around 23:40 UT and continued toward the onset, while the total magnetic field decreased, indicating an increase of cross-tail current outside of the geosynchronous orbit. Values of the T89 (Kp=5) model are also shown in the G07 data with a gray line. It can be seen that the observed field line just prior to the onset exceeded the taillike orientation of even the most taillike model. The number flux of energetic electrons decreased toward the onset over a broad energy range. These are well-known growth phase features in a geosynchronous orbit [e.g., *Kokubun and McPherron*, 1981; *Pulkkinen et al.*, 1991; *Sauvaud and Winckler*, 1980]. No apparent dipolarization and injection signatures can be seen before the onset, which suggests that this substorm was the first one after the SC. A significant change in the magnetic field variation and a significant increase of the number flux can be seen about 10 min after the onset, which indicates that the substorm disturbance region expanded to the local time of G07 and L87 around that time.

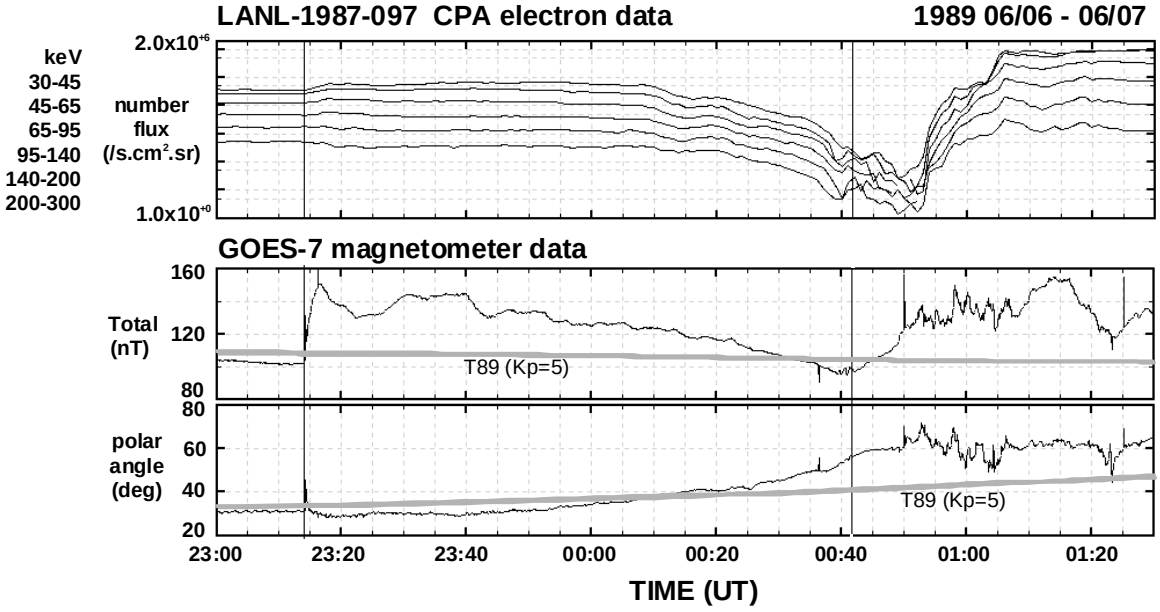

Figure 3.1.4. The number flux variation of the energetic electrons observed by L87 (upper panel) and total intensity and polar angle of geomagnetic field observed by G07 (lower 2 panels) from 23:00 UT on June 6 to 01:30 UT on June 7, 1989. Values of the T89(Kp=5) model are also shown in the G07 data panel with a gray line. Left and right vertical lines indicate the times of SC and the expansion phase onset of the substorm, respectively.

(2) Ground-based magnetic observation

Figure 3.1.5 shows the magnetic variation observed at the polar cap station, Thule (THL); at duskside and dawnside auroral latitude stations, Poste-De-La-Baleine (PBQ) and Kilpisjarvi (KIL), respectively; at auroral latitude Antarctic stations, HBA, SNA, Maitri (MAI), ASK, SYO, and Molodezhnaya (MOL); and at mid-latitude stations, Crozet (CZT) and Faraday (FAR). Unfiltered and band-pass filtered (in the Pi2 range of 40-150 sec) D-component variations of the induction magnetometer at HER are also shown in the bottom two panels. The time range in Fig. 3.1.5 is the same as that in Fig. 3.1.4. The conjugate locations of the northern hemisphere stations, THL, PBQ, and KIL are shown in Fig. 3.1.3 as small white circles. It can be seen that, before the onset, anti-sunward convection was significantly enhanced at THL, and sunward convection developed at PBQ and KIL, which suggests development of the DP-2 type two-cell convection [*Nishida*, 1968]. Looking at the data from Antarctic stations before the onset, a negative H-component variation was observed at stations eastward from SNA, whereas a positive variation was observed at HBA, which suggests that stations east of SNA were located in the morning-side convection cell and HBA was in the evening-side convection cell. After the onset, development of the westward electrojet was observed earlier at stations closer to the breakup region, HBA, SNA, and MAI, and later at stations further east, ASK, SYO, MOL, and KIL, which indicates azimuthal expansion of the substorm disturbance region corresponding to the auroral bulge evolution in Fig. 3.1.2. Positive and negative variations in the D-component at CZT and FAR after the onset indicates development of the downward and upward field-aligned currents (FACs) of the substorm current wedge (SCW) system at the eastern and western sides of the breakup region [e.g., *McPherron et al.*, 1973]. Magnetic pulsations at HER were clearly enhanced after the onset, both in the Pi2 range and at higher frequencies. All these magnetic variations show that this substorm was the first one which occurred after the SC, and the growth phase of this substorm was clearly defined.

Figure 3.1.6 shows magnetic Z-component variations at Antarctic stations. Comparing with the H-component variations in Fig. 3.1.5, the peak location of the westward equivalent current (eastward convection), indicated with upward arrows in Fig. 3.1.6, gradually moved westward and/or equatorward from MOL to MAI before the onset.

(3) Onset timing

Magnetic variations at HBA, SNA, FAR, and HER, and the intensity of the aurora observed by ATV-UV during 00:37-00:47 UT are shown in Figure 3.1.7. The temporal resolutions of the magnetic observations at HBA, SNA, FAR, and HER were 1 sec, 1 min, 20 sec, and 1 sec, respectively. The total integrated intensity and the maximum intensity of the auroral emission were calculated within the area of 18-06 hr MLT and 55-80 deg ILAT for emissions above a background threshold value. The onset time of Pi2 magnetic pulsations

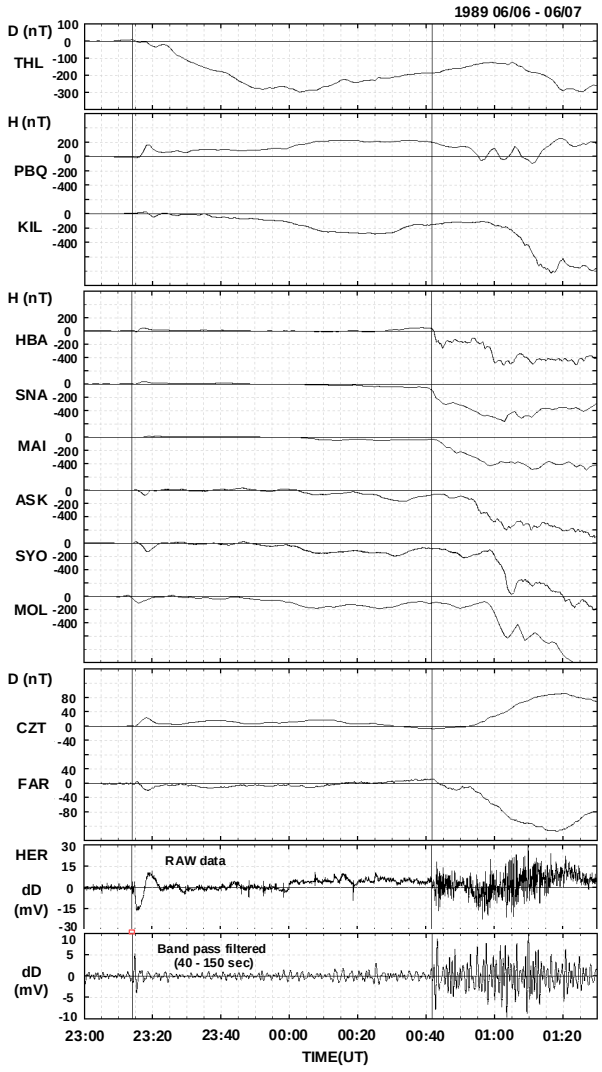

Figure 3.1.5. Observations from 23:00 UT on June 6 to 01:30 UT on June 7, 1989. From top: magnetic D-component variation at nightside polar cap station, THL; H-component at duskside (PBQ) and dawnside (KIL) auroral latitude stations; H-component at Antarctic auroral latitude stations on the nightside; D-component at dawnside (CZT) and duskside (FAR) Antarctic mid-latitude stations; D-component and the D-component filtered for Pi2 range pulsations from the induction magnetometer at HER. The two vertical lines indicate the time of SC, 23:14 UT, and the onset time, 00:41:40 UT, respectively.

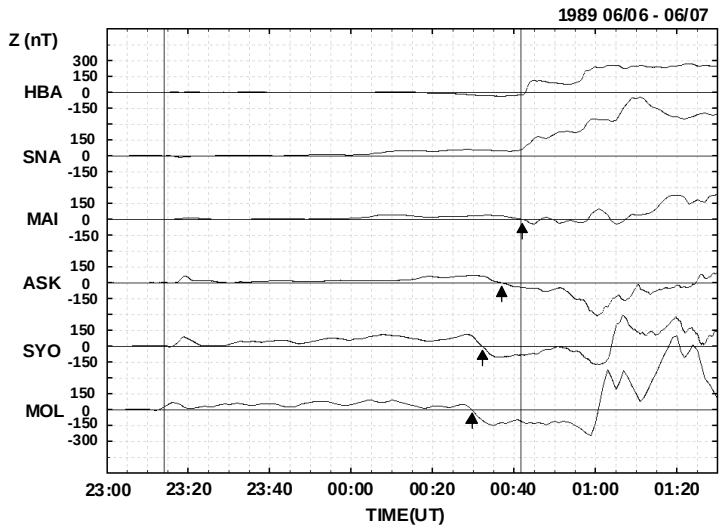

Figure 3.1.6. Magnetic Z-component variations at Antarctic auroral latitude stations on the nightside from 23:00 UT on June 6 to 01:30 UT on June 7. Two vertical lines indicate the time of SC, 23:14 UT, and the onset time, 00:41:40 UT, respectively. The upward black arrow indicates the zero-crossing time from positive to negative values.

was around 00:41:30-00:41:40 UT, determined from the induction magnetometer data at HER [*K. Yumoto*, private communication]. The total intensity of auroral emission showed a clear increase from 00:41:44 UT. In the next auroral image at 00:42:24 UT, both the total intensity and maximum intensity significantly increased. From these data, we determined the onset time of this substorm as 00:41:40 UT, which is in the range of the estimated Pi2 onset time and is between the ATV-UV observation at 00:41:36 UT and 00:41:44 UT. Around that time, the westward electrojet started to develop both at HBA and SNA. The decrease in the H-component at HBA started about 50 sec earlier, a clear decrease in the D-component at FAR started about 40 sec later, and a clear intensification of the Pi2 pulsations at HER started about 40-50 sec later. Detailed timing of these phenomena will be discussed in a second paper.

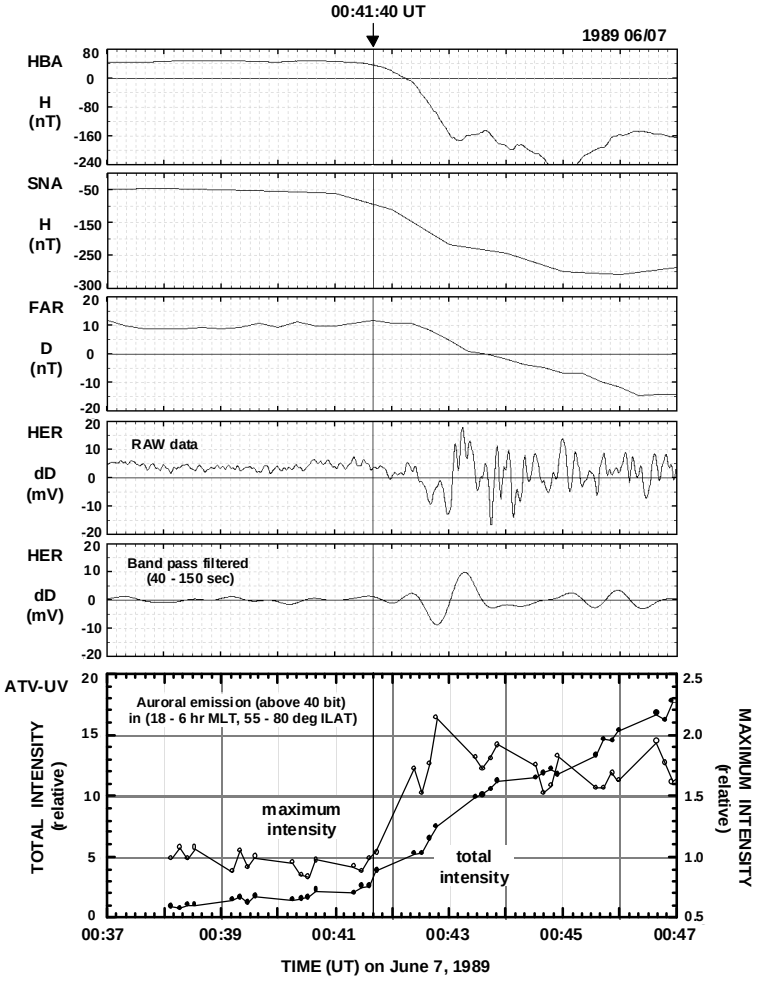

Figure 3.1.7. Observations from 00:37 UT to 00:47 UT. From top: magnetic H-component variation at HBA and SNA; magnetic D-component at FAR; D-component and the D-component filtered for Pi2 range pulsations from the induction magnetometer at HER; total integrated intensity (black circle) and maximum intensity (white circle) of UV auroral emission observed by ATV-UV within the area of 18-06 hr MLT and 55-80 deg ILAT. The vertical line indicates the determined onset time.

(4) Auroral observation at Syowa and Asuka stations

Figures 3.1.8 (a) and (b) show the MSP data at ASK and SYO, respectively. In each panel, ILAT vs time is shown for emissions at the three wavelengths, 557.7, 630.0, and 486.1 nm, assuming the emission altitudes as 120, 250, and 120 km, respectively. The latitudinal range of the 120 km (250 km) projection is 62.0-69.2 (59.8-72.8) deg ILAT at ASK and 63.0-70.4 (60.9-73.9) deg ILAT at SYO for elevation above 10 deg. Observations started at ASK at 23:21:33 UT on June 6, 1989.

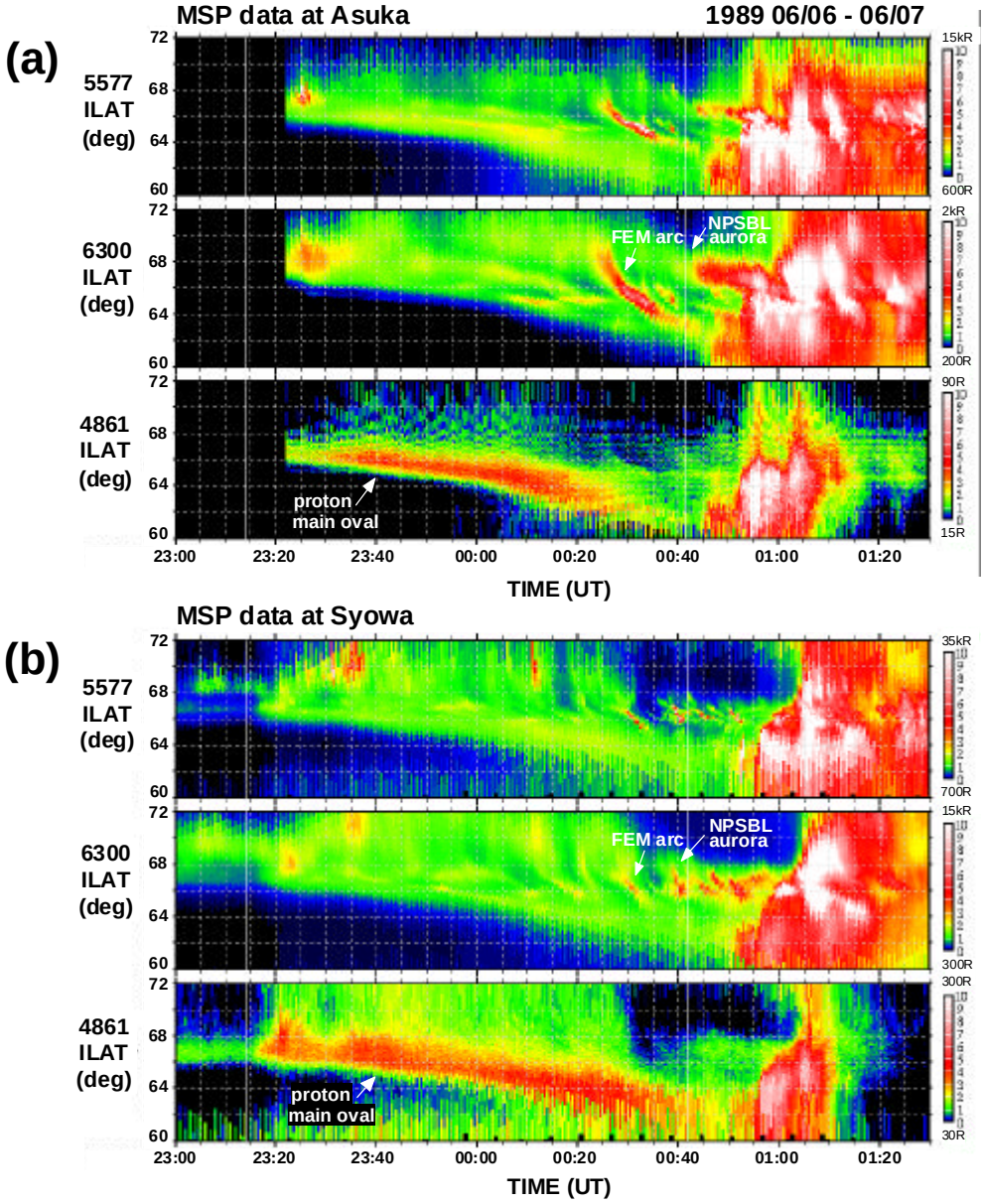

Figure 3.1.8. Three auroral emission lines (557.7, 630.0, 486.1 nm) of the MSP at ASK (a) and SYO (b) from 23:00 UT on June 6 to 01:30 UT on June 7, 1989. Left and right vertical lines indicate the times of the SC and expansion phase onset of the substorm, respectively.

After the SC, emission intensity at SYO was enhanced and the enhanced emission region spread poleward. From around 23:30 UT, the equatorward edge of the auroral region gradually moved equatorward, which was observed both at ASK and SYO at all wavelengths, most clearly at 486.1 nm. Hereinafter we call the intense equatorward-most part of the 486.1 nm emission the "proton main oval". The Average equatorward speeds of the proton main oval during 23:30-00:20 UT were 115 m/s and 92 m/s at ASK and SYO, respectively. Such a gradual equatorward motion of the auroral oval is a typical auroral feature during the growth phase [e.g., *Fukunishi*, 1975b; *Murphree et al.*, 1991; *Brittnacher et al.*, 1999]. The equatorward motion accelerated from around 00:00 UT. The average speed during 00:00-00:20 UT was 166 m/s and 117 m/s at ASK and SYO, respectively. The equatorward edge of the proton main oval moved further equatorward and was beyond the observable range of the MSP after around 00:20 UT. In the course of the growth phase, the proton main oval was always located at the equatorward-most part of the entire auroral region, both at ASK and SYO. Intensity ratios of 557.7 nm and 630.0 nm to 486.1 nm (not shown here) were nearly constant within the proton main oval during the growth phase, which suggests that those emissions were largely due to proton precipitation [e.g., *Eather*, 1968]. Such a spatial relationship between proton and electron auroral regions is typical of that observed around midnight before the expansion phase onset [e.g., *Fukunishi*, 1975b].

Around 00:22 UT (about 20 min before the onset), a discrete auroral structure appeared in the poleward region of the electron auroral data and was most evident at 630.0 nm at ASK, as indicated with a white arrow. It then moved equatorward with a higher speed than the proton main oval. Its equatorward motion gradually slowed as it approached the proton main oval. The average equatorward speed was 1.06 km/s during 00:25-00:29 UT, 0.47 km/s during 00:29-00:38 UT, and 0.22 km/s during 00:38-00:41 UT. At first its emission intensity was increasing, but it then decreased toward the onset. Hereinafter, we call it the "Fast Equatorward Moving (FEM) arc". The FEM arc can be identified also in the MSP data at SYO in Fig. 3.1.8(b), as indicated with a white arrow in the 630.0 nm data, though its structure was less clear. It became discernable later and became very weak earlier at SYO, compared with the data at ASK.

Another notable electron auroral activity feature appeared in the poleward-most region around 00:38 UT (about 4 min before the onset) both at ASK and SYO, more clearly at SYO, which is indicated with another white arrow in the 630.0 nm data. This activity continued at the same latitudes, around 66-68 deg ILAT, even after the onset. Poleward of this activity both electron and proton emissions were quite weak. The poleward boundary of 630.0 nm emission is usually considered to be very close to the polar cap boundary [*Blanchard et al.*, 1997]. Hence this activity should be located very close to the region of the plasma sheet boundary layer (PSBL) and hereinafter, we call this activity the "NPSBL (Near PSBL) aurora". At ASK, the NPSBL aurora was clearly intensified about 2 min after the onset, as can

be seen in the 630.0 nm data. A significant local poleward expansion at ASK and SYO started at lower latitudes, away from the NPSBL aurora, around 00:52 UT and 00:56 UT respectively, and a further poleward expansion beyond the latitudes of the NPSBL aurora started around 01:00 UT and 01:03 UT, respectively. Such a systematic delay from ASK to SYO matches the eastward expansion of the global auroral bulge, as shown in Fig. 3.1.2.

Contamination by scattered light from the snow surface appeared at the lowest and highest latitudes (i.e. at lowest elevation angle) in the MSP data. It can be more clearly seen in the shorter wavelength data in Fig. 3.1.8. Such contamination should be less significant at other latitudes (at higher elevation angle).

The two-dimensional characteristics of the FEM arc and the NPSBL aurora were observed by the SIT-TV camera at SYO. Figure 3.1.9 shows the SIT-TV data from 00:28:00 UT to 00:43:40 UT with 20 sec resolution. In each image, top and right are the magnetic poleward and eastward directions, respectively. Due to the characteristics of the camera lens system, the intensity at the centre of the image is weaker than the surrounding area. It can be seen that a discrete arc appeared from the western side, and extended to the center of the FOV from 00:28:00 UT to 00:30:20 UT. Its latitudinal width was about 30 km at 120 km altitude. At first its intensity increased, and then decreased as it moved equatorward. This is the FEM arc. From its equatorward motion it should still be located within the FOV of the SIT-TV camera at 00:36:00 UT, and the camera sensitivity is enough to image it. Hence, such an intensity decrease is considered to be mainly due to actual weakening of the emission intensity.

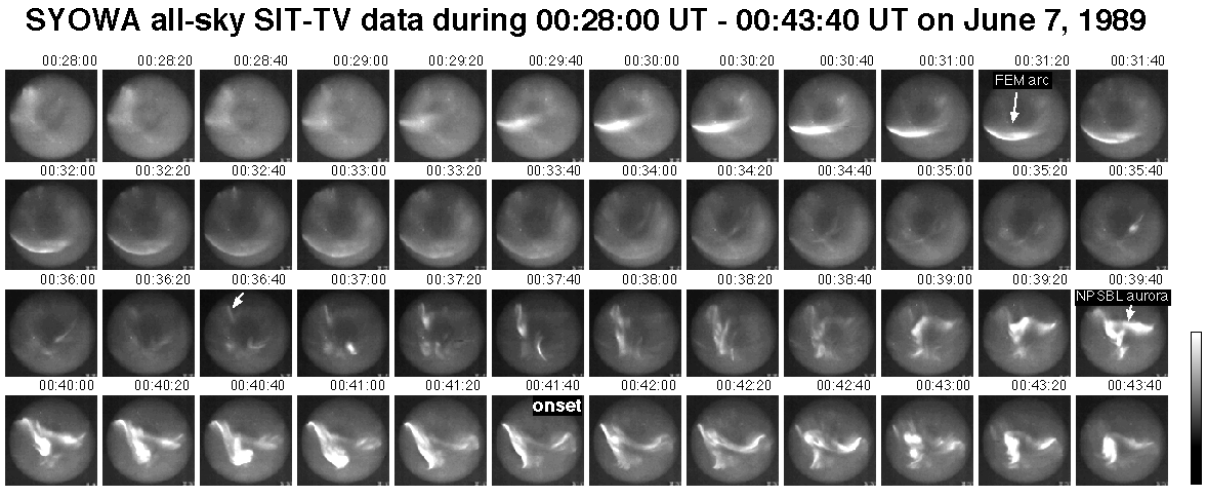

Figure 3.1.9. All-sky SIT-TV camera data at SYO from 00:28:00 to 00:43:40 UT on 7 June, 1989 at 20 sec intervals. The top and right of each image are magnetic poleward and eastward directions, respectively.

After the weakening of the FEM arc, further activity started to appear at the poleward side, as indicated with a white arrow in the image at 00:36:40 UT. It developed into a north-south

aligned form from 00:36:40 UT to 00:38:00 UT, and then an eastward branch appeared from 00:38:40 UT to 00:39:40 UT. Such a complicated structure was basically maintained after that time, even after the onset. This is the NPSBL aurora. It is apparent that the NPSBL aurora is a distinctly different auroral activity from the FEM arc.

(5) Plasma flow observation by Halley HF-radar

Figure 3.1.10 shows the ILAT-time plot of the LOS velocity for beam 8 of the Halley HF-radar. The color scale for the velocity is shown on the right-hand side. Black-to-red and black-to-blue colors indicate the velocities of plasma moving poleward and equatorward, respectively, and the two horizontal lines indicate the latitudinal range where the HF backscatter should be returned from the E-region (100-130km altitude). The data gap during 23:49 UT on June 6 - 00:00 UT on June 7 is due to an observation mode change (nearest range change).

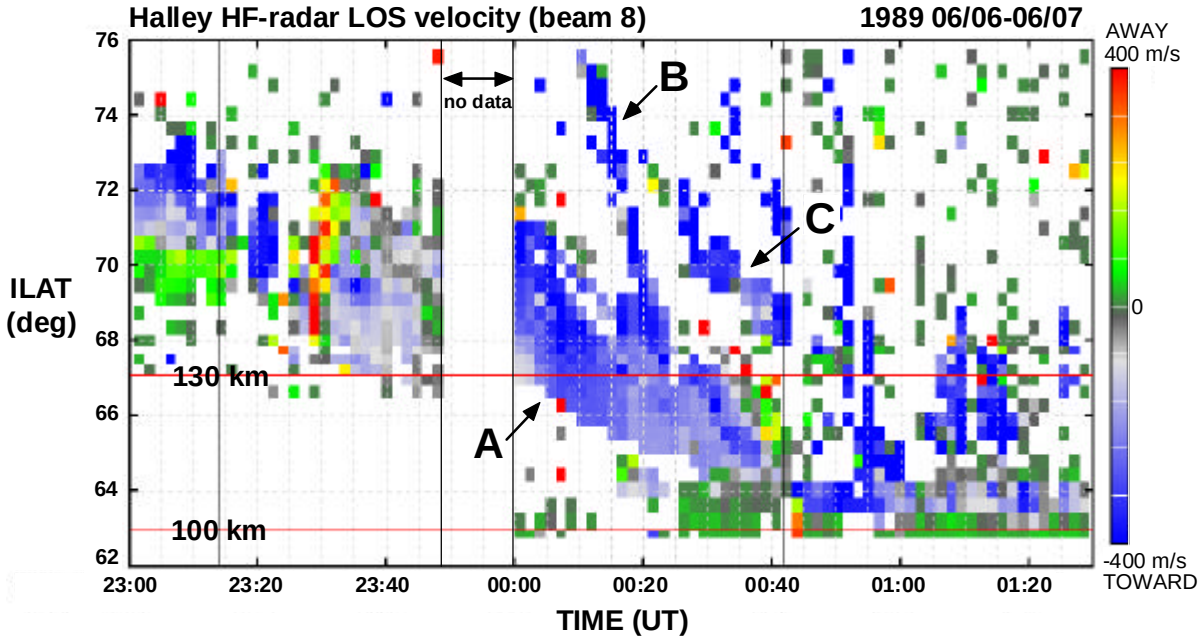

Figure 3.1.10. Observation by the Halley HF-radar from 23:00 UT on June 6 to 01:30 UT on June 7, 1989. This is an ILAT vs time plot of the line of sight velocity for beam 8. The color scale for the velocity is shown on the right-hand side. Black-to-red and black-to-blue colors indicate the velocities of plasma moving away (poleward) from and toward (equatorward) the observer, respectively. Two horizontal lines indicate the ILAT range where the HF backscatter should be returned from the altitudes of 100km-130km. Vertical lines at 23:14 UT and 00:41:40 UT indicate the times of the SC and expansion phase onset of the substorm, respectively.

It can be seen that three characteristic backscatter regions existed during the growth phase. They are indicated by arrows A, B and C. The most equatorward scatter region (A) gradually moved equatorward during the growth phase. This is a typical growth phase signature in HF-radar data [e.g., *Lewis et al.*, 1998]. Region (B) appeared around 00:11 UT at higher

latitudes, and moved equatorward with greater speed than the main region (A). Equatorward speeds of regions (A) and (B) were about 0.2 km/s and 1.0 km/s during 00:00 UT - 00:20 UT and 00:10 UT - 00:18 UT, respectively. Such contrasting equatorward motions of low and high latitude scatter regions can also be seen in the events of *Lewis et al.* [1998]. Another region (C) appeared around the time when the region (B) almost merged with the higher latitude edge of region (A). These three regions had a longitudinally extended form within the entire FOV of the HF-radar (not shown here). Plasma flows within those three regions were mainly in the equatorward direction after 00:00 UT on June 7. Poleward directed flows appeared around 65-67 deg ILAT several minutes before the onset.

Figure 3.1.11 shows the evolution of the two-dimensional flow pattern in the lower latitude part of the HF-radar FOV from 00:27:16 UT to 00:44:52 UT. In each panel, L-shell fitted flow vectors are overlapped with the LOS velocity distribution. The L-shell fitting technique assumes a constant velocity along an L-shell line to estimate the two-dimensional flow vector from the single station LOS velocity observation [*Ruohoniemi et al.*, 1989]. The validity of the L-shell fitting technique was examined critically by *Freeman et al.* [1991]. Its validity in the E-layer was examined by *Yeoman et al.* [1992]. The phase velocity in the E-layer tends to be limited by the ion acoustic velocity [e.g. *Kofman and Nielsen*, 1990], which might cause some errors in the result of the L-shell fitting technique.

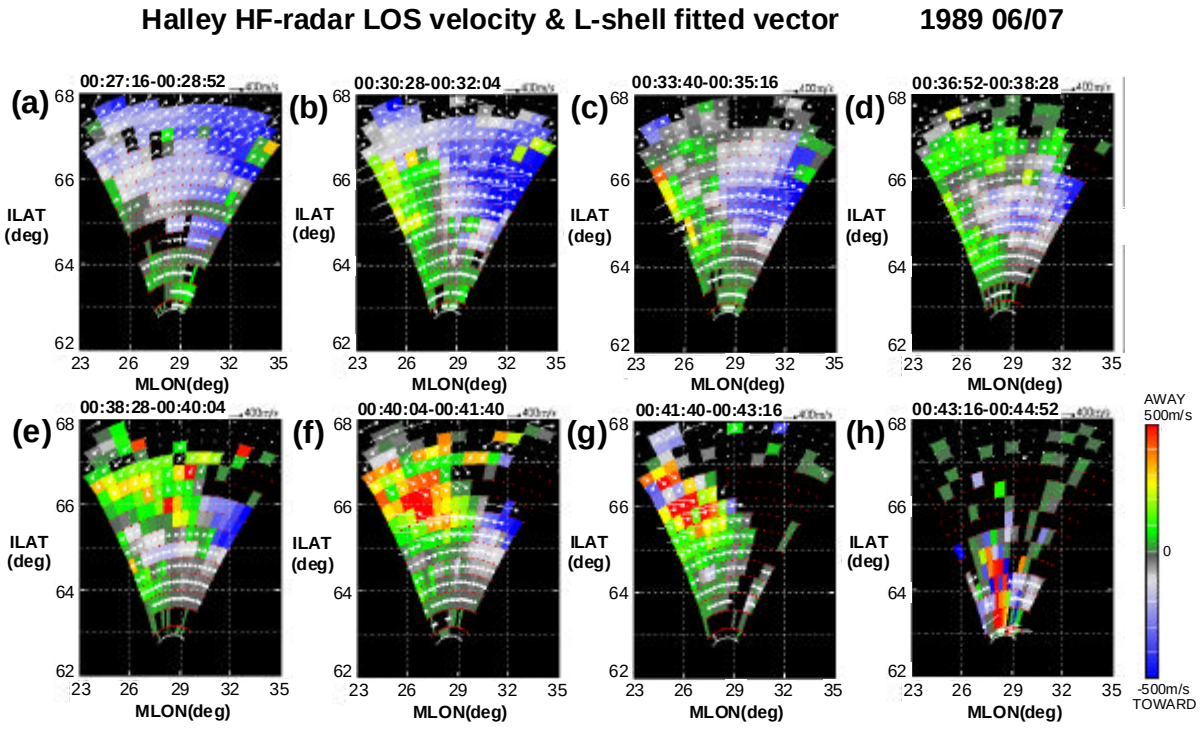

Figure 3.1.11. The two-dimensional flow pattern in the lower latitude part of the HF-radar FOV from 00:27:16 UT to 00:44:52 UT. L-shell fitted flow vectors overlap the LOS velocity distribution.

The flow pattern changed from equatorward and westward in panel (a) to intense westward flow in panels (b) and (c). Note that the westward flow was characterized by a LOS velocity distribution such that toward and away flows exist separately in the eastern and western parts of the FOV, respectively. This westward flow pattern gradually weakened and changed into a poleward and clockwise flow pattern from panel (d) to (g). Onset occurred at the beginning of the scan in panel (g).

(6) Spatial and temporal relationship between observations

(6.1) Two-dimensional evolution

Next we look at the relationship between the various observations described above. Figure 3.1.12 shows the evolution of these data from 00:28:25 UT to 00:42:24 UT on June 7, 1989 in ILAT vs MLT polar coordinates.

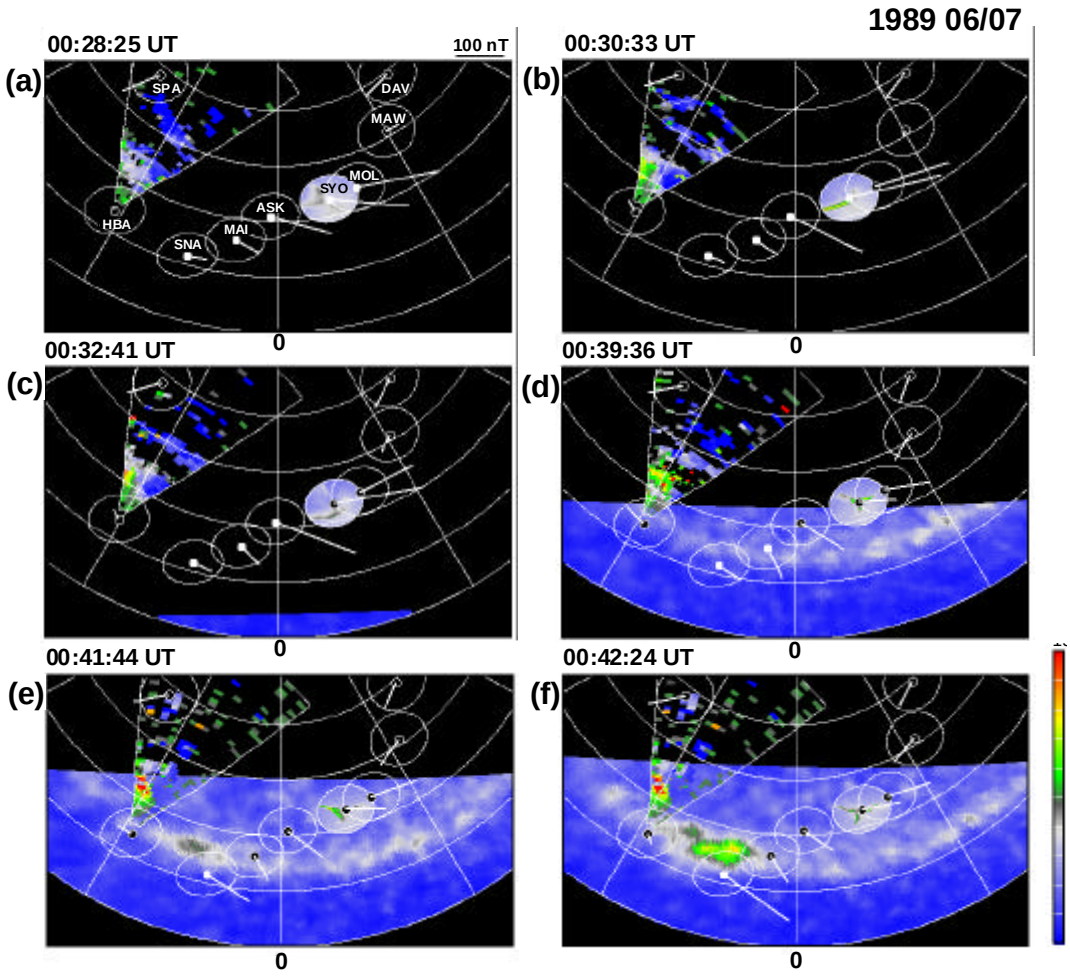

Figure 3.1.12. Two-dimensional evolution of various phenomena from 00:28:25 UT to 00:42:24 UT on June 7, 1989 in ILAT vs MLT polar coordinates at 120 km. Equi-ILAT lines are drawn at 5 deg intervals from 55 deg, and equi-MLT lines are drawn at 2 hour intervals. The FOV of ATV-UV starts from panel (c). The distribution of the LOS velocity is shown in the FOV of the Halley HF-radar, and auroral activity observed by the SIT-TV camera is shown in the FOV of SYO. The equivalent flow vector at each station is also drawn. The color code for the HF-radar data is used for all of the two-dimensional data.

Each panel shows the data at each time of the ATV-UV observation. The LOS velocity distribution from the FOV of the Halley HF-radar is shown, and SIT-TV data are shown in the FOV of SYO. The white bar with a small circle at each station shows the equivalent flow vector, derived by rotating the horizontal magnetic variation vector anti-clockwise by 90 deg. A black or white circle at each station shows positive (downward) or negative (upward) variation of the magnetic Z-component, respectively, in the mapping of the northern hemisphere image. Magnetic variations were calculated by subtracting the values at 23:00:00 UT on 6 June, 1989, the values before the SC and before the growth phase. Magnetic data are linearly interpolated, and both the HF-radar data and the SIT-TV data at the closest time are shown.

In the first panel (a), it can be seen that stations located east of SNA were in the region of the morning-side convection cell. From the Z-component variation, the peak of the eastward return flow of the convection cell was located between Mawson (MAW) (downward deflection) and MOL (upward deflection). In the second panel (b), the FEM arc appeared in the FOV of SYO, and westward flow developed in the Halley HF-radar FOV, as already shown in Fig. 3.1.11, and at HBA. Hence both the HF-radar FOV and HBA were in the region of the evening-side convection cell. Eastward return flow was enhanced at SYO and ASK, and its peak location was now between MOL and SYO, hence shifted equatorward. Further equatorward motion of the FEM arc and the peak of the return flow can be seen in the next panel (c), the peak location was between SYO and ASK at that time. Such an equatorward shift of the flow peak location was also indicated in Fig. 3.1.6, and the temporal evolution in Fig. 3.1.12 suggests that the equatorward shift proceeded concurrently with the equatorward motion of the FEM arc. As shown in Fig. 3.1.11, the flow pattern in the HF-radar FOV also showed a gradual change during the corresponding period. The peak flow location shifted further equatorward in the following panels (d) to (e). It can be seen in panel (e) that the auroral breakup occurred around the demarcation region between the morning-side and evening-side convection cells, within the UV auroral oval in the pre-midnight sector. At that time, the peak flow location of the morning-side convection cell was around the latitude of the auroral breakup.

The spatial extent (half-width) of the breakup region was 0.6 hr MLT in local time and 1.7 deg in latitude, and its peak intensity was located at 62.7 deg ILAT and 22.9 hr MLT. The latitudinal extent (half-width) of the UV auroral oval at the time of panel (e) was 61.3-63.4 deg ILAT and 60.7-62.8 deg ILAT at the ASK and SYO meridians, respectively. Comparing with the MSP data in Fig. 3.1.8, it seems likely that the UV auroral oval should be located at higher latitudes than the proton main oval at the ASK meridian, and be overlapping it at the SYO meridian at that time.

In the last panel (f), the bright region has intensified and expanded in the pre-midnight region. The eastward flow at SNA was clearly enhanced, and the flow direction at HBA

changed from westward to eastward, which indicates a development of the westward electrojet in the substorm current system. As shown in Figures 3.1.5 and 3.1.6, the center of the westward electrojet was initially located around the latitude of MAI.

In panel (d), the NPSBL aurora appeared in the FOV of SYO in the post-midnight region, and a poleward flow pattern appeared in the FOV of the Halley HF-radar around the same latitudes in the pre-midnight region. Considering the observation of the NPSBL aurora at ASK, as shown in Fig. 3.1.8, the local time distribution of the NPSBL aurora extended, at least, from midnight to the post-midnight region. Such a local time extent was very different from the pre-midnight localized breakup region.

(6.2) Comparison with satellite observations

Figure 3.1.13 shows the spatial and temporal relationship among the auroral activity, HF-radar observation, and low altitude satellite observations in the ILAT-time plot. The trajectories of AKEBONO, NOAA-10, and DMSP-F9 satellites, and the L-shell fitted flow vectors for beam 8 of the Halley HF-radar are shown together with the 630.0 nm (panel (a)) and 486.1 nm (panel (b)) MSP data at ASK. The satellite locations in panels (a) and (b) are projected to 250 km and 120 km altitude, respectively, by using the T89(Kp=0) model. As for the DMSP-F9 data, the footprints are calculated by tracing the model magnetic field-lines from the northern hemisphere to the southern hemisphere. Since field-line tracing largely depends on the external field model, we also show the results for the case of the T89(Kp=5) model, where the external field configuration is more taillike. The footprint latitudes calculated with the T89(Kp=5) model are higher than those with the T89(Kp=0) model.

The invariant latitudes of all these data were adjusted to the values at the breakup local time, 22.9 hr MLT, from the value at the MLT of each observation, by using the following equation for the ion precipitation boundary, b2i, by *Newell et al.* [1998]:

$$ILAT(cal) = ILAT(obs) - 4.31 \times \left\{ 1 - \cos\left(\pi\left(MLT(obs) - 23.4 \right) / 12 \right) \right\} \qquad (1)$$

The precipitation boundary b2i is defined by *Newell et al*. [1996] as the location of the energy flux maxima for precipitating ions above 3 keV. This boundary nearly corresponds to the isotropic boundary (IB) of 30 keV-80 keV ions for the NOAA satellite observation [e.g., *Newell et al.*, 1998; *Sergeev et al.*, 1993a], and should be located around the central region of the proton main oval observed by the MSP. Hence the MLT dependence of the b2i latitude in Eq. (1) should be nearly the same as the MLT dependence of the magnetic latitude of the proton main oval. It is not appropriate to apply Eq. (1) to phenomena at higher latitudes. In this case, local time separation between ASK-AKEBONO, ASK-DMSP-F9, and ASK-NOAA-10 was 0.23, 0.33, and 0.07 hr, respectively, when these satellites observed the open/close boundary, and the latitudinal adjustment values from Eq. (1) are very small (0.03,

0.08, and 0.01 deg, respectively). Hence, it can be considered that applying Eq. (1) to the entire latitude span in Fig. 3.1.13 should not cause a serious error in the discussion about the spatial relationship between the auroral activity observed at ASK and precipitation boundaries observed by the satellites.

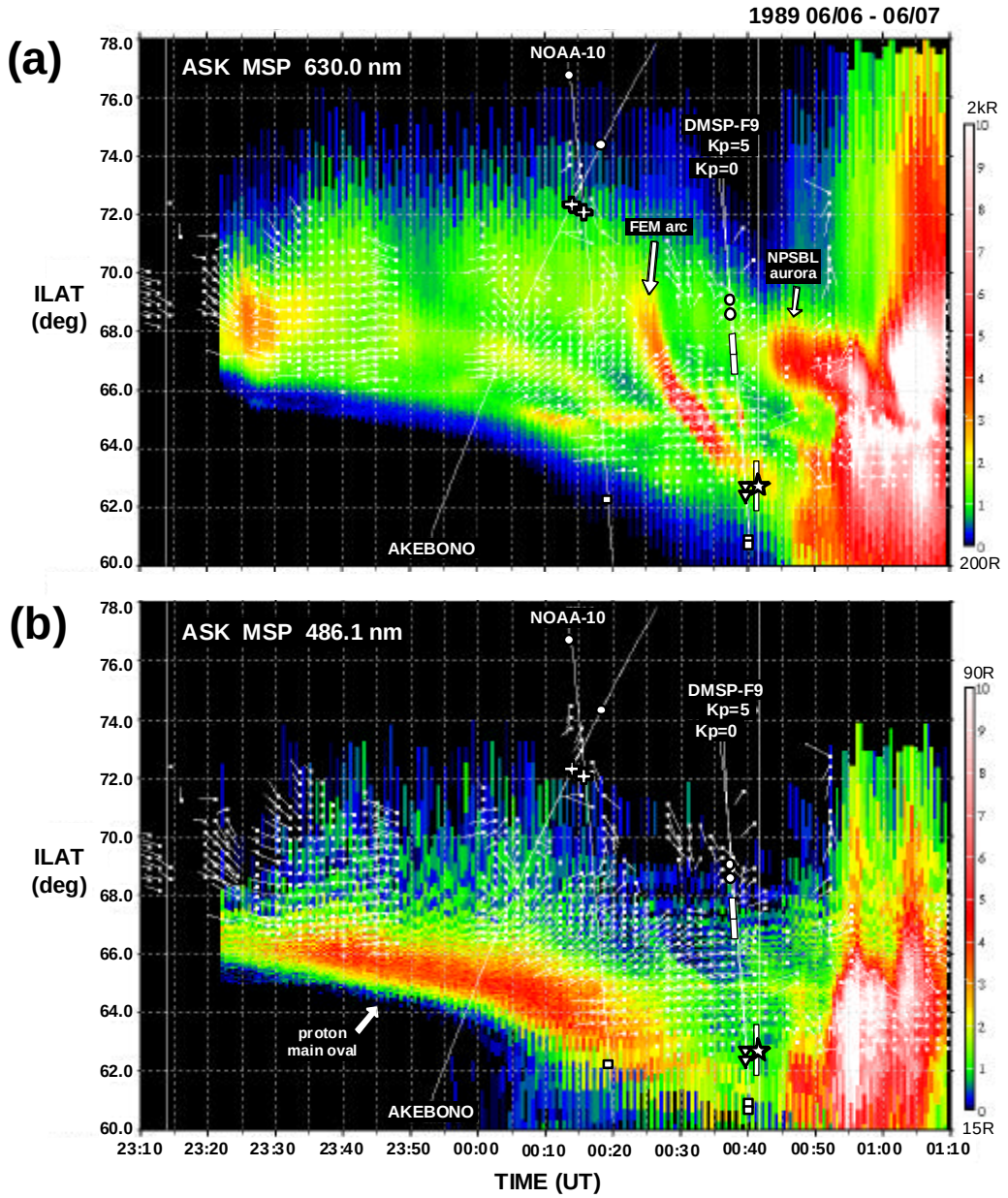

Figure 3.1.13. A combined ILAT vs time plot of various observations from 23:10 UT on June 6 to 01:10 UT on June 7, 1989. The 630.0 nm (upper panel) and 486.1 nm (lower panel) MSP data at ASK, the L-shell fitted flow vector for beam 8 of the Halley HF-radar, and footprint trajectories of AKEBONO, NOAA-10, and DMSP-F9 satellites are shown. Footprints of AKEBONO and NOAA-10 are calculated with the T89(Kp=0) model, and that of DMSP-F9 is calculated with the T89 model in Kp=0 and 5 conditions. Latitudes of these observations are adjusted to the values at the UV auroral onset local time (22.9 hr MLT) by using Eq. (1) (see text for detail). White circles, open/close boundary; White crosses, apparent change in electron energy flux; White squares, ion isotropic boundary & b2i boundary; Inverse white triangles, inverted-V type electron precipitation; White bars along DMSP-F9 orbit, enhanced electron energy flux; White star, UV auroral onset latitude; White bars along the onset time line, latitudinal half width of the UV auroral breakup region.

Fig. 3.1.13 does not indicate a direct mapping of the HF-radar data from the HBA meridian to the onset local time, but shows a possible latitudinal relationship between the backscatter region and the auroral distribution at the HBA meridian by adjusting the latitudes of both phenomena. Furthermore, since the local time separation between ASK and HBA is rather large (about 2.0 hr), auroral activity which has a strong MLT dependence (such as the FEM arc) might not appear at the HBA meridian in the same form as at ASK. For such auroral activity, Fig. 3.1.13 should be considered as showing a possible relative latitudinal and temporal relationship between the HF backscatter region at the HBA meridian and auroral activity at ASK, hence between different phenomena at different local times. The latitudinal adjustment between HBA and ASK from Eq. (1) is 0.99 deg to 0.16 deg for the period from 23:10 UT to the onset time.

White circles on the satellite trajectories indicate the open/close boundary. White crosses on the trajectories of AKEBONO and NOAA-10 indicate locations where the precipitating electron energy flux shows a clear enhancement (going equatorward). The white bar on the DMSP-F9 trajectory indicates a region of enhanced energy flux of precipitating electrons. The poleward edge of the white bar corresponds to the boundary b5e of *Newell et al.* [1996], which indicates the poleward edge of the electron auroral oval. A white cross should be put at the poleward edge, but it is omitted to avoid complication. White squares on the trajectories of NOAA-10 and DMSP-F9 indicate the IB of 30 keV-80 keV ions and the b2i boundary, respectively. A white inverse triangle on the DMSP-F9 trajectory indicates the location of the most-equatorward inverted-V type electron precipitation. The white star and white bar on the vertical line at the onset time show the latitudes of the peak intensity and half-width of the UV auroral breakup region, respectively.

It is clear that the open/close boundary shifted equatorward during the growth phase with a higher speed than the equatorward motion of the proton main oval. The FEM arc initially appeared at the poleward side of the entire auroral region, close to the interpolated latitude of the poleward edge of the enhanced electron energy flux, and then moved equatorward toward the proton main oval with a higher speed than the open/close boundary. In other words, its relative location within the entire auroral region shifted from the poleward side to the more equatorward side. The FEM arc did not intrude into the proton main oval. Its equatorward motion was gradually slowed, and it was located at the poleward edge of the proton main oval just prior to the onset. Its latitude became very close to that of the most-equatorward inverted-V type electron precipitation observed by DMSP-F9 and the UV auroral breakup latitude. The breakup occurred about 6 deg equatorward of the open/close boundary, about 2 deg poleward of the b2i boundary, and poleward of the proton main oval. The poleward edge of the NPSBL aurora was very close to the open/close boundary, and its central part was very close to the enhanced electron energy flux observed by DMSP-F9. The correspondence between the NPSBL aurora and those precipitation characteristics is better shown by the

T89(Kp=5) model than the T89(Kp=0) mapping. We can expect that the satellite footprints should shift further poleward along the trajectory, because the external field configuration just prior to onset should become even more taillike than represented by the T89(Kp=5) model, as shown in Fig. 3.1.4.

It can be seen that the main backscatter region (A) in the HF-radar data was situated on the high latitude side of the proton main oval, and equatorward shifts of both the backscatter regions (B) and (C) were followed by the FEM arc and the NPSBL aurora, respectively. These observations indicate a close temporal relationship between the three characteristic auroral activities and the three characteristic HF backscatter regions.

Figure 3.1.14 shows the data obtained by the three low altitude satellites, AKEBONO (panel (a)), NOAA-10 (panel (b)), and DMSP-F9 (panel (c)). In each panel, the latitude increases towards the right. Precipitation boundaries and regions shown in Fig. 3.1.13 are indicated in each panel. In the AKEBONO data, the top two panels are for the energy-time (E-t) plots of the precipitating electrons and ions (pitch angle range of 120-180 deg) in the energy range 13 eV-16.4 keV and 16 eV-20.1 keV, respectively. The bottom panel is for the precipitating total energy flux of electrons (black line) and ions (blue line). Details of the instrument for the low energy particles (LEP) are described in *Mukai et al.* [1990]. Equatorward of the open/close boundary, both electron and ion total energy fluxes increase. The white cross marks a secondary increase of the electron total energy flux. A clear inverted-V type precipitation can be seen around 00:13 UT, equatorward of the marked location. Between the open/close boundary and the marked location, an intense beam like ion precipitation exists, showing a slight energy dispersion such that the precipitation energy increases in the poleward direction during 00:14:30-00:16:00 UT. Such characteristics in the precipitating particles are typical ones which can be observed around the PSBL region [e.g., *Fukunishi et al.*, 1993], and the energy dispersed ion precipitation pattern is usually termed VDIS.

In the NOAA-10 data, the top and third panels are for the total energy flux of precipitating electrons and ions in the energy range of 0.3 keV-20 keV, respectively. The second and bottom panels are for the count rates of precipitating (black) and trapped (blue) electrons and ions in the energy ranges of > 30 keV and 30 keV-80 keV, respectively. Details of the SEM (Space Environment Monitor) instruments of NOAA satellites are described in *Hill et al.* [1985]. Similar to the AKEBONO data, both electron and ion total energy fluxes increase equatorward of the open/close boundary. The white cross marks a secondary increase of the electron total energy flux. Ion IB is defined as the most-equatorward location of the isotropic region, where the count rate of precipitating energetic ions is equal to that of the trapped ones.

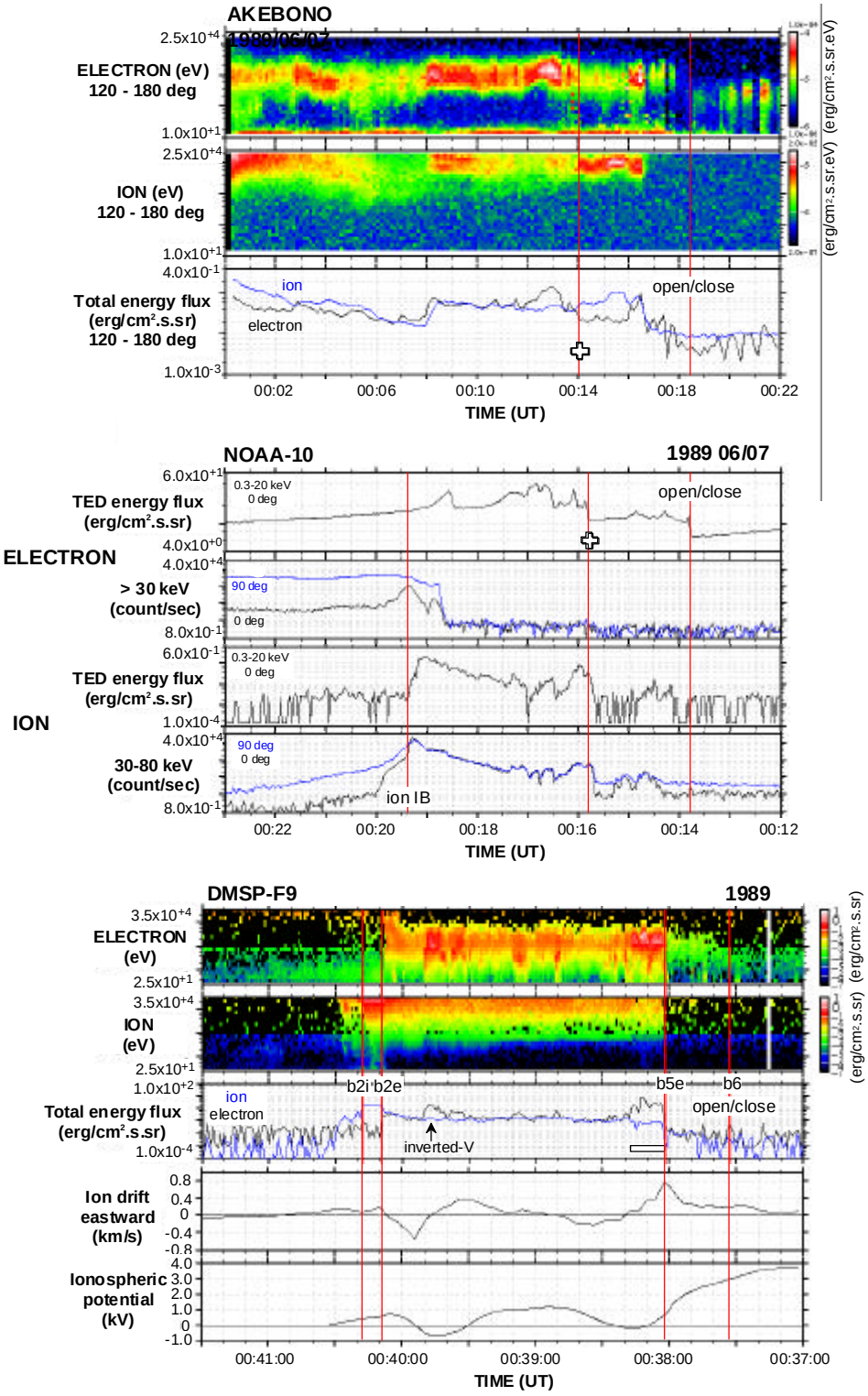

Figure 3.1.14. (a) AKEBONO data. From top: energy-time (E-t) plots for the precipitating electrons and ions; precipitating total energy flux. (b) NOAA-10 data. From top: precipitating electron (0.3-20 keV) total energy flux; electron (> 30 keV) count rate for two pitch angles (0 and 90 deg); precipitating ion (0.3-20 keV) total energy flux; ion (30-80 keV) count rate for two pitch angles (0 and 90 deg). (c) DMSP-F9 data. From top: E-t plots for the precipitating electrons and ions; total energy flux for the precipitating electrons and ions; leftward (eastward) cross-track ion drift speed observed by the ion driftmeter; ionospheric potential along the satellite track, calculated from the ion drift data. In each panel, left and right are lower and higher latitudes, respectively. Specific boundaries and features, which are shown in Fig. 13, are also indicated.

In the DMSP-F9 data, the upper two panels are the E-t plots of the precipitating electrons and ions, respectively, in the energy range of 31 eV-31.3 keV. The third panel is for the total energy flux of electrons (black) and ions (blue). The bottom two panels are for the leftward (nearly eastward in this case) cross-track ion drift speed and calculated electrostatic potential along the satellite track, respectively; these are obtained by the ion driftmeter. Note that the rightward increasing (decreasing) gradient in the ion drift data corresponds to the negative (positive) potential regions. Details of the particle detectors are described in *Hardy et al.* [1984], and details of the driftmeter data are introduced on the Web page [*http://utd500.utdallas.edu/~hairston/sept99.html*]. We adopted the b6 boundary by *Newell et al.* [1996] (boundary between the subvisual drizzle and polar cap precipitation) as the open/close boundary. The other boundaries by *Newell et al.* [1996], b5e, b2e, and b2i are also indicated. The b5e and b2e are defined as follows: b5e, Poleward edge of the electron main oval, where the electron total energy flux drops-off by a factor of 4 between the previous and succeeding 12 sec averaged values; b2e, Earthward edge of the plasma sheet electrons. On both equatorward and poleward sides of this boundary, the average electron energy decreases. An enhanced total energy flux of precipitating electrons, indicated with a white bar, can be seen just equatorward side of the b5e boundary. This enhanced flux region corresponds to a negative potential region. A positive potential region exists on the poleward side between the b5e and b6 boundaries, and a large eastward flow (equatorward electric field) exists between the two potential regions. These are typical characteristics observed around the PSBL region [e.g., *Fukunishi et al.*, 1993; *Yamamoto et al.*, 1993; *Burke et al.*, 1994]. The most-equatorward inverted-V type electron precipitation around 00:39:40 UT-00:39:50 UT is indicated with an upward arrow. The b2i boundary is located equatorward of the b2e boundary, and the ion precipitation region extended more equatorward than the electron precipitation region, which matches the spatial relationship between the proton and electron auroral distributions observed by the MSP, as shown in Fig. 3.1.13.

3. Discussion

3.1. Growth phase evolution in the ionosphere

A summary of the observations and our interpretation of the evolution of the ionospheric phenomena observed during the growth phase of this substorm are shown schematically in Figure 3.1.15. During the growth phase, both the open/close boundary and the equatorward edge of the proton main oval gradually moved equatorward. The speed of the equatorward movement of the former was greater the latter, hence the latitudinal width of the auroral region gradually decreased. This is a typical feature of growth phase evolution [e.g., *Brittnacher et al.*, 1999; *Friedrich et al.*, 2001]. About 20 min before the onset (about 40 min after the start of the growth phase), the FEM arc appeared on the poleward side of the auroral region (Fig. 3.1.15(a)). It moved equatorward toward the proton main oval with a greater

speed than the open/close boundary. Its equatorward motion gradually slowed as it approached the proton main oval (Fig. 3.1.15(b)). Eventually, just prior to the onset, the FEM arc was almost in contact with the high latitude edge of the proton main oval (Fig. 3.1.15(c)).

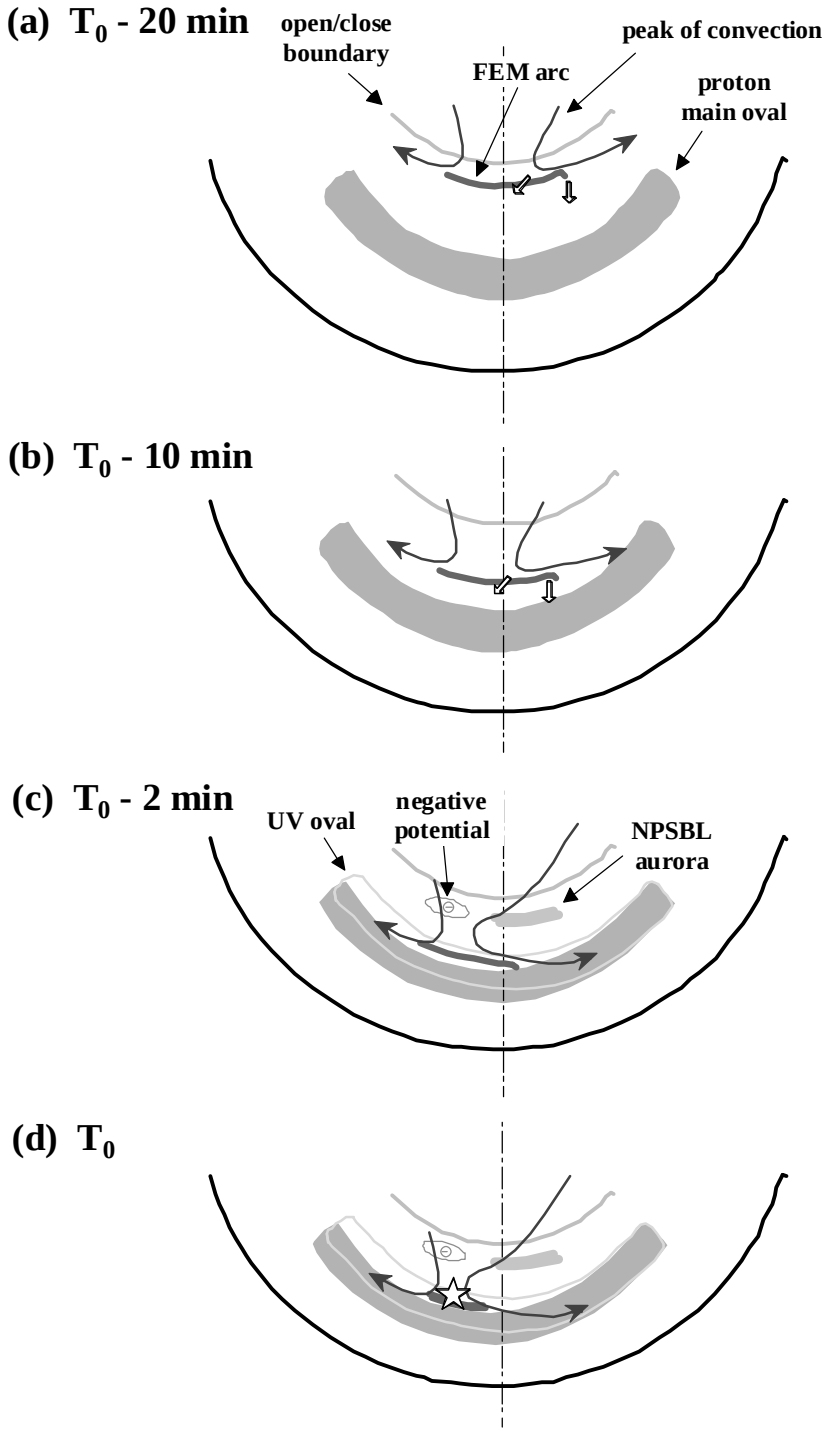

Figure 3.1.15. Schematic drawing of the evolution of the ionospheric phenomena observed during the growth phase of this substorm. Four panels show the situation at four selected times before the onset time, T0.

The UV auroral oval, observed by ATV-UV, was located at latitudes higher than the proton main oval around the breakup meridian, as can be supposed from the latitudinal relationship between the breakup region and the proton main oval in Fig. 3.1.13(b). UV auroral breakup occurred in the pre-midnight sector within the UV auroral oval at latitudes very close to the FEM arc (Fig. 3.1.15(d)) as shown in Figures 3.1.12 and 3.1.13. The peak location of the breakup was (62.7 deg ILAT, 22.9 hr MLT), and its local time extent was about 0.6 hr MLT for the half-width. Such a pre-midnight breakup is consistent with previous observations [e.g., *Frank and Craven*, 1988; *Murphree et al.*, 1991; *Elphinstone et al.*, 1995a], and the peak location was within the range of the average values given by *Elphinstone et al.* [1995a], (65.9 ± 3.5 deg ILAT, 22.9±1.2 hr MLT). Note that the breakup latitude in this event was close to the lowest value of the above range, which indicates a well-developed growth phase evolution. The local time extent of the breakup region in this event was a little narrower than the average value, 1 hr, of *Elphinstone et al.* [1995a].

As shown in Figures 3.1.13 and 3.1.14, the breakup occurred at latitudes very close to the FEM arc and the equatorward-most inverted-V type electron precipitation, and at the high latitude edge of the proton main oval, about 2 deg poleward from the ion isotropic boundary. Such an observation concerning the onset location is basically consistent with previous results [e.g., *Akasofu*, 1964; *Elphinstone et al.*, 1995a; *Vallance Jones et al.*, 1982; *Deehr*, 1994; *Deehr and Lummerzheim*, 2001].

As shown in Fig. 3.1.8, the FEM arc was observed more clearly at ASK than at SYO. Its intensity increased first, and then decreased toward the onset. Such a "fading" of the FEM arc was observed earlier at SYO. Considering the longitudinally extended form of the FEM arc as shown in Fig. 3.1.9, we suggest that such a "fading" should occur from its eastern edge, and then propagates further westward. Based on such a consideration, we show in Fig. 3.1.15 the longitudinal extent of the FEM arc as gradually decreasing and its central meridian gradually shifting toward the onset meridian as it moved equatorward. In other words, the longitudinal extent of the FEM arc reduced and eventually was localized around the onset region at onset time.

A few minutes before the onset, when the FEM arc was almost in contact with the proton main oval, the NPSBL aurora clearly appeared in the most poleward region (Fig. 3.1.15(c)). Almost simultaneously with the appearance of the NPSBL aurora, a clock-wise flow pattern appeared within the FOV of the Halley HF-radar around the latitudes of the NPSBL aurora, as shown in Figures 3.1.11, 3.1.12 and 3.1.13. This clock-wise flow pattern suggests that a negative potential region should appear at the eastern side of it as depicted in Fig. 3.1.15(c) and (d). DMSP-F9 data shown in Fig. 3.1.14(c) indicate that the NPSBL aurora should correspond to an enhanced energy flux of precipitating electrons and a negative potential in the poleward-most region. The observations at SYO and ASK, by DMSP-F9 and the Halley HF-radar suggest that the negative potential region corresponding to the NPSBL aurora might

extend from the meridian of SYO to the eastern side of the Halley HF-radar FOV, i.e., in the local time range of about 22.5 hr - 01 hr MLT. The NPSBL aurora cannot be identified clearly in the ATV-UV data. This is possibly because of the coarse spatial resolution of the ATV-UV. UV auroral breakup occurred at latitudes about 4-5 deg equatorward from the NPSBL aurora. The local time extent of the UV auroral breakup, 0.6 hr, was much narrower than the estimated longitudinal extent of the NPSBL aurora. Clearly the local time extent of the NPSBL aurora was very different from that of the breakup region. This suggests that the process responsible for localization of the breakup region has little relationship with the source mechanism for the NPSBL aurora.

Samson et al. [1992a] showed two events where breakup occurred 4 and 6 deg equatorward of the open-closed field line boundary, which was estimated by the poleward edge of the 630.0 nm emissions. *Friedrich et al.* [2001] analyzed eight events, including the two events of *Samson et al.* [1992a], and also showed a similar spatial relationship between the breakup latitude and the open-closed field line boundary at the onset time. Our result in this study is consistent with these previous observations. The breakup latitude in this event, 62.7 deg, is much lower than in their cases (average latitude of about 67 deg).

The peak velocity of the nightside return flows of the two-cell ionospheric convection moved equatorward simultaneously with the equatorward motion of the FEM arc, although the large scale convection pattern itself did not show a significant change, as shown in Fig. 3.1.12. Just prior to the onset, the velocity peak was located at latitudes close to the UV auroral breakup, and the breakup occurred around the demarcation region of the two-cell convection as shown in Fig. 3.1.12. A similar spatial relationship between the breakup location and the nightside convection demarcation region can be inferred from Plate 2 of *Lu et al.* [2000] and from comparison between Plates 2 and 3 of *Fedder et al.* [1995].

In this event, equatorward motion of the return flow peak was observed for the morning-side convection cell, and was unclear for the evening-side convection cell, although the flow pattern within the FOV of the Halley HF-radar showed some change simultaneously with the equatorward motion of the FEM arc, as shown in Figures 3.1.10, 3.1.11, 3.1.12, and 3.1.13. Hence equatorward motion of the return flow peak for the evening-side convection cell depicted in Fig. 3.1.15 is our speculation and should be confirmed in future observations. *Voronkov et al.* [1999] showed that the maximum of the westward flow (which should be the return flow of the evening-side convection cell) intensified, moved equatorward and followed the proton aurora band during the growth phase. A significant latitudinal gradient in the convective flow developed within the proton aurora region prior to the onset. It is suggested that their observation of the evening-side convection cell could be a counter-part of our observation of the morning-side convection cell. Since *Voronkov et al.* [1999] used MSP data along a single meridian, the spatial relationship between that meridian and the location of global expansion phase onset was not clear.

3.2. FEM arc

Evolution of the FEM arc and its relationship to the proton main oval and the onset location in this study are very similar to the case of the 'contact breakup' in *Oguti* [1973]. Similar fast equatorward motion of electron discrete aurora from the poleward-most region toward the proton auroral region during the growth phase can be seen, for example, in Fig. 3.1.3 in *Lyons et al.* [1997], and in Fig. 3.1.1 in *Friedrich et al.* [2001], although it is not discussed by them. *Deehr and Lummerzheim* [2001] analyzed in detail the evolution of the proton and electron auroral arcs during the growth phase. In their one event, two different kinds of electron arcs appeared at latitudes higher than the "hydrogen arc" during the growth phase: one was a "hard electron arc", characterized by lower values of 630-nm/558-nm emission ratio, and the other was a "soft electron arc", characterized by the higher emission ratio. The former existed from the beginning, while the latter clearly appeared about 10 min before the onset, and at latitudes higher than the former and became the "onset arc". Hence, their "onset arc" was not the equatorward-most arc. They showed that the peak hydrogen emission moves equatorward quicker than does the onset arc. However, looking at their Figure 3.1.2, the "onset arc" moved equatorward with a similar speed to the "hydrogen arc". They focused on only the peak emission, and gave little consideration to the whole region. If we consider the whole region, including the weak diffuse region in their Plate 1, it can be supposed that the "hard electron arc" moved from the poleward side of the diffuse region to the middle of it during the growth phase and became the equatorward-most arc. Comparing with our observation, the characteristics of the FEM arc in our event are similar to those of the "hard electron arc" in *Deehr and Lummerzheim* [2001].

Local breakup starting with an intensification of the equatorward-most arc is often observed at the westward end of the auroral bulge in association with westward expansion of the bulge, while poleward expansion at the eastward end of the bulge has different characteristics [e.g., *Akasofu*, 1964; *Fukunishi*, 1975b; *Vallance Jones et al.*, 1982]. From only ground-based observation, it is generally very difficult to determine whether the observed breakup is a local or global one, and whether the equatorward-most arc is actually the onset arc related to the global initial breakup. On the other hand, the spatial resolution of a satellite imager is generally not enough to resolve the discrete structure of the onset arc. To our knowledge, there are very few examples showing that the global auroral breakup, observed by a satellite imager, occurred at the equatorward-most onset arc, as observed at the ground. In this event, the latitude of the global initial breakup was very close to that of the FEM arc and the equatorward-most inverted-V type electron precipitation observed by DMSP-F9, as seen in Fig. 3.1.13(a). Since there were no ground-based observations of the FEM arc at the breakup local time and the field-line tracing of the DMSP-F9 data from the northern hemisphere has a level of uncertainty, we cannot say definitely that the FEM arc did

eventually become the onset arc in the global sense.

It is generally understood that the equatorward motion of the auroral region during the growth phase is mainly caused by the configuration change of the magnetospheric field lines toward a more taillike one [e.g., *Sergeev et al.*, 1990]. The greater equatorward velocity of the open/close boundary than that of the proton main oval suggests that the taillike configuration change should proceed more rapidly in the more tailward region or in the higher latitude region in the tail, especially during the early stage of the growth phase. The FEM arc, relative to the whole auroral region, moved from the poleward side towards the equatorward edge, which suggests that its equatorward motion should be caused not only by such a tail configuration change, but also by an actual earthward approach of the source region in the tail. Deceleration of the equatorward motion of the FEM arc suggests that the earthward approach speed was slowed as it moved closer to the onset region in the magnetosphere.

It can be seen in Fig. 3.1.13 that the FEM arc initially appeared around the interpolated location of the poleward edge of the enhanced electron energy flux which was observed by AKEBONO, NOAA-10, and DMSP-F9. As shown in Fig. 3.1.14, intense beam-like ion precipitation was observed by AKEBONO between the open/close boundary and the poleward edge of the enhanced electron energy flux. Such a distribution of the electron and ion precipitation is a typical characteristic of the PSBL region [e.g., *Fukunishi et al.*, 1993], which is considered to be a low altitude projection of a very thinned region earthward of an X-type neutral line in the tail [e.g., *Burke et al.*, 1994]. Hence the equatorial projection of the FEM arc should be located around the earthward edge of the very thinned region. Continuous equatorward motion of the FEM arc from its initial appearance suggests that the source mechanism for the FEM arc remained constant. Hence it can be supposed that the source region should continue to be situated around the earthward edge of a very thinned region, and the equatorward shift of the relative location of the FEM arc suggests that the very thinned region spreads earthward in the tail.

Equatorward movement of the peak location of the return flows, which occurred simultaneously with the equatorward motion of the FEM arc, suggests that the peak locations of the duskward and dawnward flows of the sunward convection move earthward in association with the earthward motion of the source region in the tail for the FEM arc.

3.3. NPSBL aurora

In this event, the NPSBL aurora clearly appeared a few minutes before the onset. Similar intensification of the poleward-most electron auroral activity before the onset can be seen in Fig. 3.1.1 of *Samson et al.* [1992a], although they did not discuss it.

Elphinstone et al. [1995a] showed that there are some cases in which the so-called "double oval" configuration [cf., *Elphinstone et al.*, 1995b] already exists when the onset starts within the UV oval at lower latitudes, because the recovery phase of the preceding

substorm has not yet been completed or substantial activity still continues. Such an example can also be seen in Plate 2 of *Deehr and Lummerzheim* [2001]. In our case, the NPSBL aurora appeared during the growth phase of the first substorm which occurred after a long quiescent period. Hence, our case should be different from the cases of *Elphinstone et al.* [1995a].

It is also known that auroral activity, termed "Poleward Boundary Intensifications (PBI)", appears at the poleward boundary of the auroral zone [e.g., *Lyons et al.,* 1999]. In all the events of *Lyons et al.* [1999], PBI were observed during a "double oval" configuration which appeared after the expansion phase of a substorm, and they were considered to be "an important aspect of geomagnetic activity that is distinct from substorms". On the other hand, the NPSBL aurora in our study appeared during the late growth phase, and significant further poleward expansion occurred around the latitudes of the NPSBL aurora during the expansion phase, as shown in Fig. 3.1.8, which suggests that the NPSBL aurora should be closely associated with the substorm evolution. These characteristics of the NPSBL aurora are very different from those of the PBI.

As can be seen in Figures 3.1.13 and 3.1.14, the NPSBL aurora should correspond to the enhanced energy flux of precipitating electrons and a negative potential in the poleward-most region, which was observed by DMSP-F9. A positive potential region existed at its poleward side and an enhanced equatorward electric field existed between the two potential regions. Such a distribution is also a typical characteristic of the region around the PSBL [e.g., *Yamamoto et al*., 1993; *Burke et al*., 1994]. The NPSBL aurora continued to exist in the poleward-most region even after the onset. It intensified at the ASK meridian a few minutes after the onset, as can be seen in Fig. 3.1.13. These observations suggest that the source region for the NPSBL aurora should be located in a very thinned region earthward of an X-type neutral line in the tail, similar to the initial location of the source region for the FEM arc. In contrast to the FEM arc, the source mechanism for the NPSBL aurora should become active a few minutes before the onset, and the source location relative to the X-type neutral line should not change significantly even after the onset. Hence it can be supposed that the source mechanism for the NPSBL aurora should be closely associated with the activity around the X-type neutral line.

Since there were no observations in the tail region beyond geosynchronous orbit in this event, we cannot determine definitely whether this neutral line is the distant neutral line (DNL) or the near earth neutral line (NENL). There are many event studies and statistical studies showing that the initial formation of the NENL often starts around X=-20 to -30 Re about 1 to 5 min before the ground-based Pi2 onset [e.g., *Sergeev et al*., 1995; *Mukai et al*., 1998; *Ohtani et al*., 1999; *Nagai et al*., 1998; *Nagai and Machida*, 1998; *Machida et at*., 1999; *Miyashita et al*., 2000]. Previous statistical studies also showed that the velocities of the fast earthward and tailward flows from the NENL clearly increase soon (about 1-2 min) after the Pi2 onset [e.g. *Nagai and Machida*, 1998; *Machida et al*., 1999; *Miyashita et al*., 2000],

which indicates an activation of the NENL soon after the onset. About 10 min after the onset, a plasmoid develops explosively [*Machida et al.*, 2000], which indicates further activation of the NENL. As for the DNL, *Machida et al.* [2000] showed that activation of the earthward flow from the DNL (X ~ -130 Re) starts at least 20 min prior to the Pi2 onset, and the earthward flow disappeared about 10 min after the onset, which suggests a quenching of the reconnection at the DNL. Comparing such a temporal evolution of the NENL and DNL with evolution of the NPSBL aurora in this event, it is more probable that the X-type neutral line responsible for the NPSBL aurora should be the NENL. Hence our observation of the NPSBL aurora could be the first report showing a possible auroral signature of the NENL formation before the onset in the tail.

3.4. Growth phase evolution in the magnetosphere

Our interpretation for the evolution in the magnetosphere, based on the above discussions, is schematically shown in Figure 3.1.16. Left and right columns in Fig. 3.1.16 show the evolution in the X-Y and X-Z planes, respectively, at the four times corresponding to the four times in Fig. 3.1.15. During the early stage of the growth phase, a taillike configuration change of the plasma sheet field-lines proceeds more rapidly in the region close to the DNL. The source region for the FEM arc is located around the earthward edge of a very thinned region. Initially, its location is distinctly separated from the source region for the proton main oval in the near earth region (Fig. 3.1.16(a)). About 40 min after the growth phase starts (about 20 min before the onset), the taillike configuration change starts to accelerate from the down tail region toward the near earth region, and the source region for the FEM arc starts to move earthward, changing its relative location between the DNL and the source region for the proton main oval (Fig. 3.1.16(b)). The locations of the peak duskward and dawnward deflection flows of the magnetospheric sunward convection also move earthward simultaneously with the earthward motion of the source region for the FEM arc. In that 40 minutes, the solar wind can travel a distance of about 143 Re with its speed of about 380 km/s. Hence, after the 40 min, almost all of the closed field line region should be dominated by the negative IMF-Bz condition. The earthward spreading speed of the very thinned region and the earthward speed of the source region for the FEM arc are gradually slowed, and the azimuthal extent of the source region is gradually localized toward the pre-midnight region as it approaches the source region for the proton main oval. Just prior to the onset, the location of the source region for the FEM arc is almost fixed in space around the tailward edge of the source region for the proton main oval. The NENL starts to be formed in the near tail and the source region for the NPSBL aurora appears on the earthward side of the NENL (Fig. 3.1.16(c)). The taillike configuration change continues, and onset occurs in a pre-midnight localized region around the location close to the source region for the FEM arc, around the demarcation region between the deflection flows of the sunward

convection, and well earthward from the NENL (Fig. 3.1.16(d)).

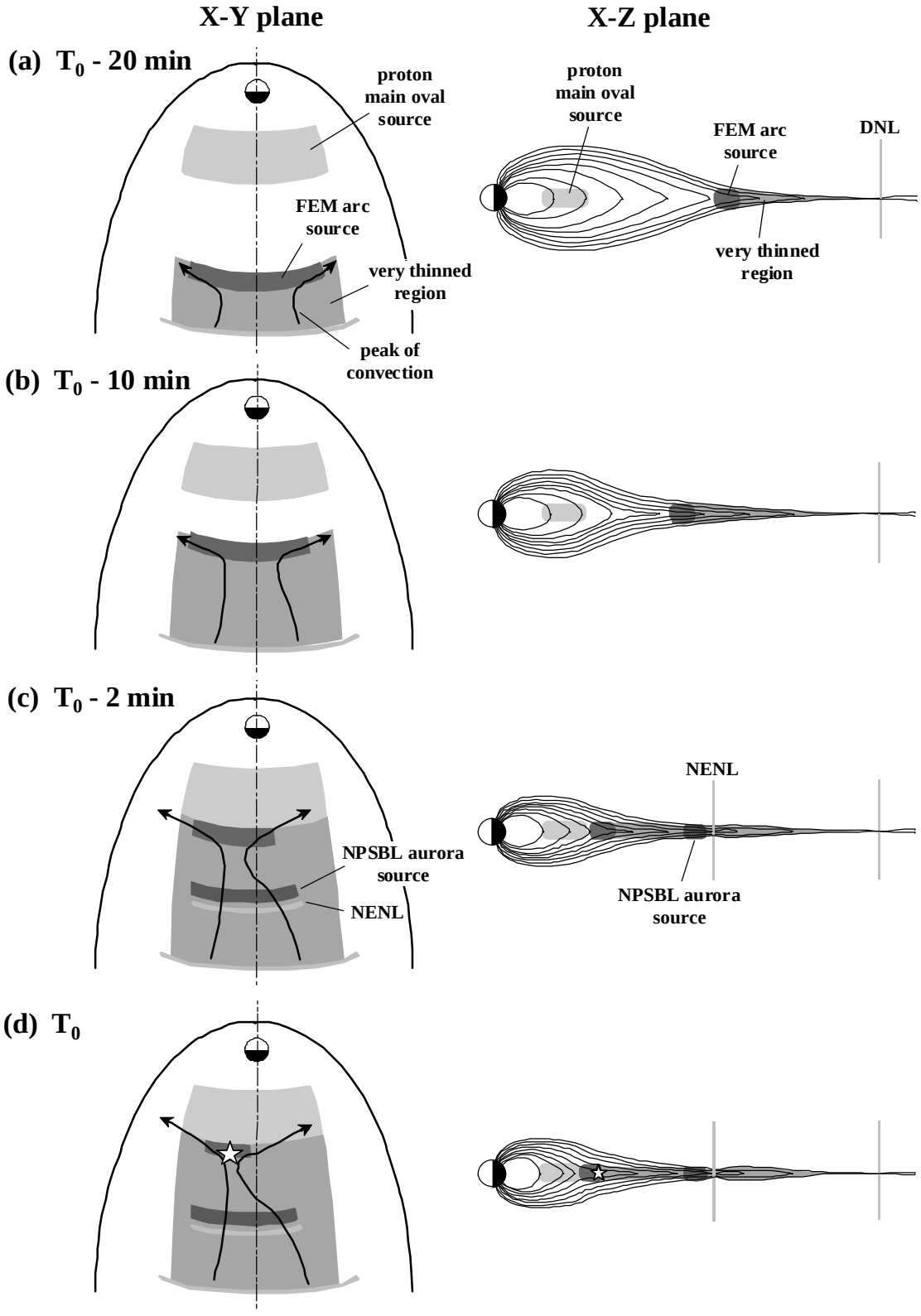

Figure 3.1.16. Schematic drawing of the growth phase evolution in the magnetosphere, corresponding to the ionospheric phenomena shown in Fig. 3.1.15.

One of the most debated topics in substorm study is the relative timing of various onset signatures, both in the ionosphere and magnetosphere. Relative timing between formation of the NENL and start of "current disruption" (CD) in the near earth region has been critical issue concerning the onset mechanism. In the NENL model, CD or dipolarization is a consequence of NENL formation [e.g., *Baker et al.*, 1996; *Birn and Hesse*, 1996], while, in the synthesis model based on the CD model, NENL formation is a consequence of a tailward propagating rarefaction wave which is excited as a result of the CD process [e.g., *Lui*, 1991a]. As already mentioned, many event studies and statistical studies have shown that the initial formation of the NENL often starts about 1 to 5 min before the ground-based Pi2 onset. *Yumoto et al.* [1989] showed that CD onset tends to be preceded by ground-based Pi2 onset by about 0-3 min. *Ohtani et al.* [1999] analyzed one event and showed that the NENL formation preceded the CD onset by about 5 min. *Lui et al.* [1998] used the auroral breakup as a mark of the onset time, and stated that their result did not show any indication of strong flows substantially (> 2 min) preceding the onsets. As for the relative timing between auroral breakups and Pi2 onsets, *Liou et al.* [2000a] showed that the Pi2 onsets tend to lag behind the auroral breakups by 1-3 min.

In our event, Pi2 onset almost coincided with the auroral breakup, as shown in Fig. 3.1.7, and the relationship between the appearance of the NPSBL aurora and the Pi2 onset seems to be consistent with the observations of NENL formation before the onset, as already discussed. Such a timing relationship does not necessarily imply a cause-and-effect relationship. As already discussed, the local time range of the NPSBL aurora was very different from that of the breakup region, which suggests that the process responsible for localization of the onset region should have little relationship with the reconnection process at the NENL, hence the onset process (or CD process) might be independent of NENL formation. Such an inference was also mentioned by *Ohtani et al.* [1999]. We suppose that the source mechanism for the FEM arc and concentration of the convective flows into a localized onset region should be closely associated with the onset mechanism and the pre-midnight localization of the onset region.

4. Summary and Conclusions

We have analyzed in detail the evolution of nightside auroral activity and ionospheric convection during the growth phase of an isolated substorm which occurred after a long quiescent period. Our detailed analysis of these phenomena provided some important evidence for understanding how the growth phase of a substorm proceeds toward the expansion phase onset both in the ionosphere and magnetosphere.

The following three characteristic auroral activities were identified: 1. proton main oval; 2. FEM arc; 3. NPSBL aurora. It was found that the evolution of the nightside convection was closely associated with the evolution of the FEM arc. UV auroral breakup occurred in a

pre-midnight localized area around the demarcation region of the two-cell convection, close to the latitudes of the FEM arc near the poleward edge of the proton main oval. Toward the onset, both the FEM arc and the peak velocity of the return flows of the two-cell convection moved equatorward. Such an evolution started about 20 min before the onset (about 40 min after the growth phase started).

The NPSBL aurora was one of our new findings in this study. It clearly appeared in the poleward-most region a few minutes before the onset, and continued to exist around the same location even after the onset. A significant further poleward expansion of the bulge occurred from the latitudes of the NPSBL aurora.

We have discussed the magnetospheric processes responsible for these ionospheric phenomena. The source region for the FEM arc should be located around the earthward edge of a very thinned region, and its equatorward motion suggests that such extreme thinning should proceed earthward during the late growth phase. The temporal and spatial evolution of the NPSBL aurora suggests that this auroral activity should be closely associated with the NENL formation. The local time distribution of the breakup region was very different from that of the NPSBL aurora, which suggests that the onset mechanism itself should be independent of NENL formation, and should be closely associated with the source mechanism for the FEM arc.

The growth phase of this substorm was well-developed. Further event studies and statistical studies should be done in the future to confirm how often and under what conditions the above-mentioned growth phase features can be observed. Well-coordinated simultaneous observations in the ionosphere and magnetosphere are necessary to study magnetospheric processes corresponding to these ionospheric phenomena.